New Insight into the Binding Mode of Peptide Ligands at Urotensin-II Receptor: Structure−Activity Relationships Study on P5U and Urantide

Paolo Grieco,[†,‡] Alfonso Carotenuto,[†,‡] Pietro Campiglia,[#] Isabel Gomez-Monterrey,[‡] Luigia Auriemma,[‡] Marina Sala,[#] Cristina Marcozzi,[‡] Roberta d'Emmanuele di Villa Bianca,[||] Diego Brancaccio,[‡] Paolo Rovero,[§] Paolo Santicioli,[⊥] Stefania Meini,[⊥] Carlo A. Maggi,[⊥] and Ettore Novellino*[,‡]

Department of Pharmaceutical and Toxicological Chemistry, University of Naples "Federico II", Via D. Montesano, I-80131 Naples, Italy, Laboratorio Interdipartimentale di Chimica e Biologia dei Peptidi e Proteine, Department di Scienze Farmaceutiche, Università di Firenze, I-50019 Sesto Fiorentino, Florence, Italy, Department of Experimental Pharmacology, University of Naples "Federico II", I-80131 Naples, Italy, Department of Pharmacology, Menarini Ricerche, Via Rismpondo 12/A, I-50131 Florence, Italy, Department of Pharmaceutical Science, University of Salerno, I-84084 Fisciano, Salerno, Italy

Received February 5, 2009

Urotensin II (U-II) is a disulfide bridged peptide hormone identified as the ligand of a G protein-coupled receptor. Human U-II (H-Glu-Thr-Pro-Asp-c[Cys-Phe-Trp-Lys-Tyr-Cys]-Val-OH) has been described as the most potent vasoconstrictor compound identified to date. We have recently identified both a superagonist of *h*U-II termed P5U (H-Asp-c[Pen-Phe-Trp-Lys-Tyr-Cys]-Val-OH) and the compound termed urantide (H-Asp-c[Pen-Phe-DTrp-Orn-Tyr-Cys]-Val-OH), which is the most potent UT receptor peptide antagonist described to date. In the present study, we have synthesized several analogues of P5U and urantide in which the Asp[4] residue in N-terminus position was replaced with coded and noncoded amino acids. The replacement of the Asp[4] residue by Tic led to an analogue, compound **14**, more potent as antagonist ($pK_B = 8.94$) compared to urantide. Furthermore, a different SAR was observed for the P5U compared to the urantide analogues. NMR and docking studies revealed a different binding mode for the agonist and antagonist ligands which could explain the observed SAR.

Introduction

Urotensin-II (U-II[a]) is a cyclic peptide originally isolated from goby fish urophysis.[1] Subsequently, it has been found that U-II is also present in tetrapods and that its gene is expressed in the CNS.[2] The U-II precursor has now been cloned in various vertebrate species including frog, rat and mouse, pig, monkey, and human.[3−6] U-II was identified as the natural ligand of an orphan G-protein-coupled receptor,[7] now referred to as UT receptor.

Recently, an analogue of U-II, called urotensin-related peptide (URP), has been identified in mammals.[8] In all U-II and URP isoforms known so far, the sequence of the cyclic C-terminal hexapeptide has been fully conserved across species.[9] The U-II and URP genes are primarily expressed in motoneurons located in discrete brainstem nuclei and in the ventral horn of the spinal cord.[10−13] U-II and URP mRNAs have also been detected, although at a much lower level, in various peripheral tissues including the pituitary, heart, spleen, thymus, pancreas, kidney, small intestine, adrenal, and prostate.[3,8,14]

The U-II/UT receptor system seems to play an important role in cardiovascular functions; in fact, *h*U-II has been shown to be 1−2 orders of magnitude more potent than endothelin-1 in producing vasoconstriction in mammals and thus is one of the most effective vasoconstrictor compounds identified to date.[7,15,16] On the basis of its spectrum of activities, *h*U-II has been postulated to contribute as modulator to cardiovascular homeostasis and possibly to be involved in certain cardiovascular pathologies.[15,17] It has been recently demonstrated that U-II is involved in inhibition of insulin release[18] in the perfused rat pancreas and may play an important role in pulmonary hypertension.[19] Central nervous effects of U-II have also been described.[20] Hence, the *h*U-II ligands could be of therapeutic value in a number of pathological disorders. It has been demonstrated that the C-terminal octapeptide of U-II retains full biological activity and binding properties.[21−26]

The (patho)physiological role(s) of the U-II/UT receptor system and, most importantly, the potential interest of UT receptor ligands as drug candidates, prompted the development of low molecular weight compounds as nonpeptide UT receptor agonists and antagonists (Figure 1).[27]

Our research group has been involved for a long time in the development of UTR peptide ligands. The optimization of a peptide as a lead structure is important to improve its pharmacokinetic properties and in identifying the pharmacophore elements, that is, to determine the key amino acid residues that

* To whom correspondence should be addressed. Phone: +39-081-678646. Fax: +39-081-678644. E-mail: novellin@unina.it.
† These authors contributed equally to the work
‡ Department of Pharmaceutical and Toxicological Chemistry, University of Naples "Federico II".
§ Laboratorio Interdipartimentale di Chimica e Biologia dei Peptidi e Proteine, Department of Scienze Farmaceutiche, Università di Firenze.
|| Department of Experimental Pharmacology, University of Naples "Federico II".
⊥ Department of Pharmacology, Menarini Ricerche.
Department of Pharmaceutical Science, University of Salerno.

[a] Abbreviations: Abbreviations used for amino acids and designation of peptides follow the rules of the IUPAC-IUB Commission of Biochemical Nomenclature in J. Biol. Chem. 1972, 247, 977−983. Amino acid symbols denote L-configuration unless indicated otherwise. The following additional abbreviations are used: U-II, urotensin-II peptide; *h*U-II, human urotensin-II peptide; SDS, sodium dodecylsulphate; SAR, structure−activity relationship; NMR, nuclear magnetic resonance; DQF-COSY, double quantum filtered correlated spectroscopy; PE COSY, primitive exclusive correlated spectroscopy; TOCSY, total correlated spectroscopy; NOESY, nuclear Overhauser enhancement spectroscopy; NOE, nuclear Overhauser effect; MD, molecular dynamic; EM, energy minimization; 1D, 2D, and 3D, one-, two-, and three-dimensional; Pen, penicillamine; TSP, 3-(trimethylsilanyl) propionic acid; DMSO, dimethylsulfoxide; Orn, ornithine; IL, intracellular loop; EL, extracellular loop; TM, trans-membrane domain; Cpa, *p*-chlorophenylalanine; Tic, tetrahydroisoquinoline; Nal, naphthylalanine; *h*-UTR, human urotensin II receptor; *r*-UTR, rat urotensin II receptor.

10.1021/jm900148c CCC: $40.75
Published on Web 05/11/2009

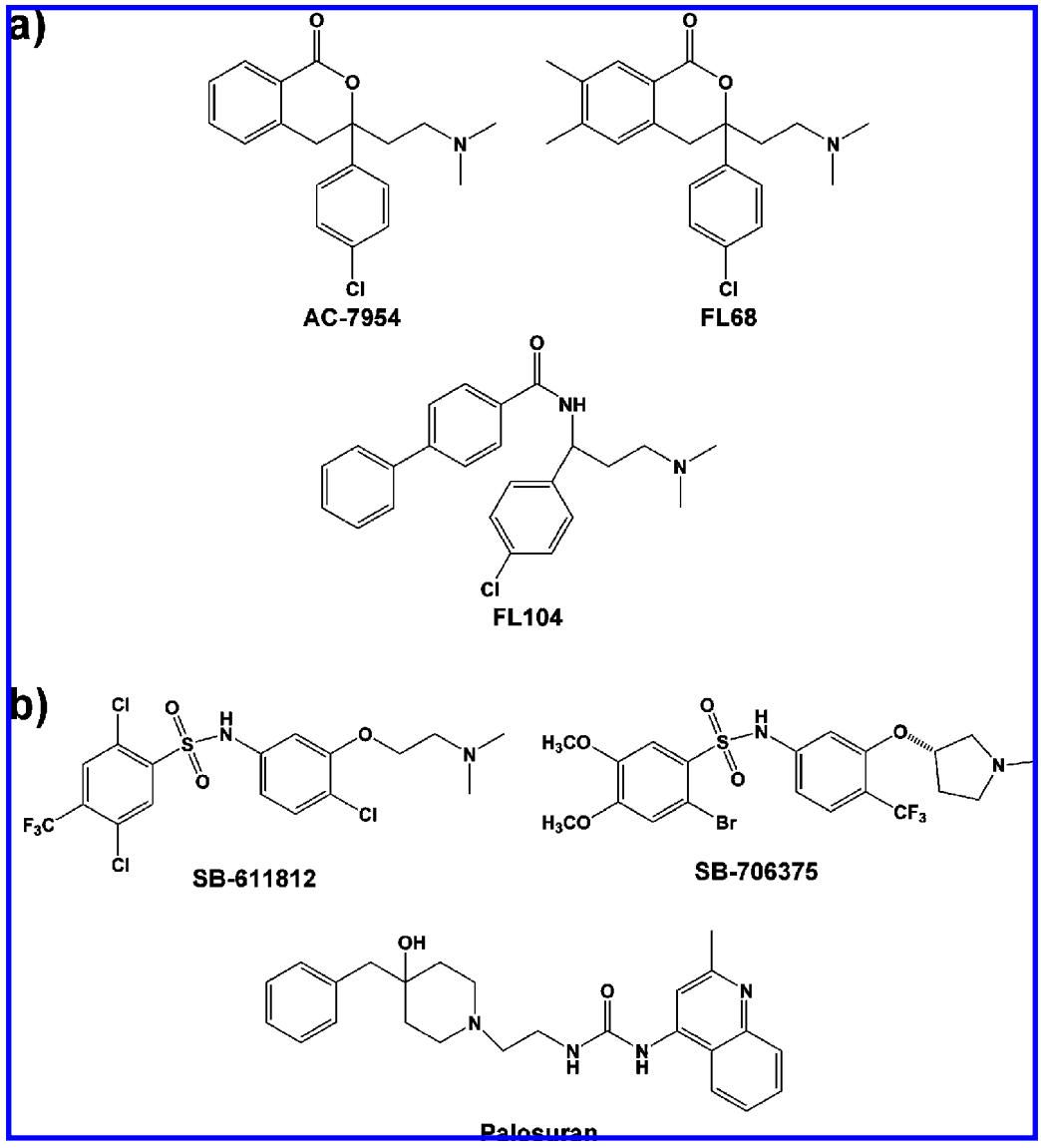

Figure 1. Some representative structures of nonpeptide UTR agonists (a) and antagonists (b).

are involved in the biological activity.[28] Interestingly, some common features are observable (two aryl moieties and a protonable nitrogen atom) in organic and peptide UTR ligands.[29] Hence, the structural information obtained by the peptide investigation might be useful for the design of both small molecules and peptide ligands.

In previous studies, we have identified both a superagonist named P5U (H-Asp-c[Pen-Phe-Trp-Lys-Tyr-Cys]-Val-OH),[30] and an antagonist, urantide (H-Asp-c[Pen-Phe-DTrp-Orn-Tyr-Cys]-Val-OH),[31] of *h*U-II. The latter is the most potent peptide antagonist at UT receptor described to date. Actually, urantide behaves as a pure antagonist in the rat aorta bioassay[31] and as a full agonist in a calcium mobilization assay performed in CHO cells expressing the *h*-UTR.[32] This point has been widely discussed elsewhere.[33] For sake of simplicity, we will refer to urantide as an antagonist throughout the manuscript.

Recently, we performed extensive NMR and computational studies on both P5U and urantide that allowed us to formulate a hypothesis about the structural changes that determine the switching from agonist to antagonist activity.[33,34]

To aim to identify new leads for the development of both agonists and antagonists at UT receptor, we have studied the structure−activity relationships of a series of novel P5U and urantide analogues based on the chemical substitution of the Asp[4] residue with several other amino acid residues with different physicochemical properties (Figure 2 and Supporting Information Figure S1). The most interesting analogues were then analyzed by NMR and their structures fitted within *h*-UTR models to gain insight into the agonist and antagonist binding modes.

Results

Chemistry. Peptides were synthesized according to the solid phase approach using standard Fmoc methodology in a manual reaction vessel[35] (Experimental Section).

The purification was achieved using a semipreparative RP-HPLC C-18 bonded silica column (Vydac 218TP1010). The purified peptide was 98% pure as determined by analytical RP-HPLC. The correct molecular weight of the peptide was confirmed by mass spectrometry and amino acid analysis (Supporting Information).

Biological Data. Receptor affinity at *h*-UTR and biological activity (rat aorta bioassay) of the synthesized compounds are reported in Table 1. Substitution of the native Asp[4] residue in

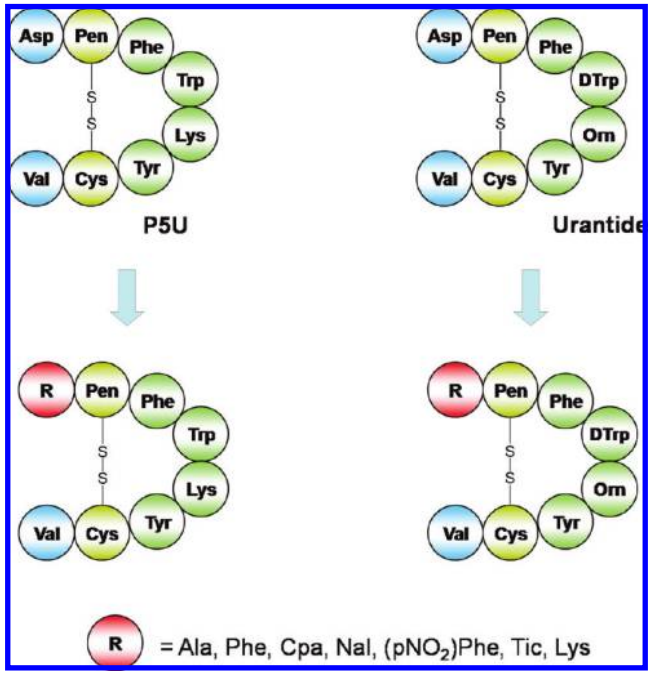

Figure 2. New synthesized compounds.

P5U by an Ala residue (compound **1**), which generated an URP analogue, slightly reduced the contractile potency of the peptide (pEC_{50} = 8.04). Similar modification in urantide sequence produced compound **2** with antagonist activity but slightly less potent than urantide (pK_B 7.84). Subsequently, to evaluate the role of an aromatic residue in position 4, we replaced Asp^4 with a Phe residue in both sequence of P5U and urantide. Compound **3** showed to be a superagonist as P5U (pEC_{50} = 9.18), while the same substitution in urantide sequence generated compound **4** with a reduced binding affinity but with an increased antagonist activity (pK_i 7.71 and pK_B 8.68). Then, the Asp^4 residue was replaced with some uncoded aromatic amino acids (Figure 2). Compound **5**, in which Asp^4 was replaced with a Cpa residue, resulted in being less potent as agonist compared to P5U (pEC_{50} 8.86). Similar trend was observed in compound **6** with a reduced antagonist potency (pK_B 7.85). Analogue **7**, containing in position 4 a Nal(1) residue, showed a sensible reduction both in binding (pK_i 7.58) and functional activity (pEC_{50} 6.99), while the same substitution in urantide sequence (compound **8**) resulted in a conserved antagonist activity (pK_B 8.50). Interestingly, Nal(2) derivative of P5U (compound **9**) regained high agonist activity (pEC_{50} 8.28). On the other hand, compound **10** resulted to be slightly less potent compared to compound **8** and urantide (pK_B 7.89).

Replacing the Asp^4 residue with the amino acid pNO_2Phe in both parent peptides led to compounds with reduction in activity. In fact, compound **11** resulted to have a reduced binding affinity at UT receptor (pK_i 7.87) and a more considerable reduction in functional activity (pEC_{50} 7.14). Compound **12**, resulted in being slightly less potent with respect to urantide, showing a pK_B of 7.90. Analogue **13**, in which Asp^4 residue was replaced with a Tic residue, showed a slightly reduced activity (pEC_{50} 8.87). Surprisingly, the same substitution in urantide sequence produced analogue **14** with increased antagonist potency, showing a pK_B value of 8.94. This compound represents a new potent antagonist discovered by this study. Finally, the replacement of Asp^4 with a Lys residue in P5U (analogue **15**) resulted in a reduced activity (pEC_{50} 8.22). Worthy of note, the same modification in urantide sequence produced an analogue (compound **16**) showing a dramatic reduction in binding affinity and antagonist activity (pK_i 6.66 and pK_B 7.49), being by far the weakest ligand among the synthesized compounds.

NMR Analysis. A whole set of 1D and 2D NMR spectra in 200 mM aqueous solution of SDS were collected for compounds **14** and **16**. These peptides were chosen because **14** is the most potent antagonist of the series, while **16** has very low binding affinity and antagonist potency (Table 1). Micelle solution was employed because we have recently reported the NMR structure of UT agonists (among which is P5U)[34] and antagonist (among which is urantide)[33] in this medium.

Complete ^1H NMR chemical shift assignments were effectively achieved for the two peptides according to the Wüthrich procedure[36] via the usual systematic application of DQF-COSY,[37] TOCSY,[38] and NOESY[39] experiments with the support of the XEASY software package (Supporting Information).[40] Peptides **14** and **16** differs from urantide only for the N-terminal residue substitution and show diagnostic NMR parameters (H_α proton chemical shifts, NOE contacts, $^3J_{NH-H\alpha}$ and $^3J_{H\alpha-H\beta}$ coupling constants, NH exchange rates and temperature coefficients) all similar to those observed in the parent peptide (Supporting Information). In particular, NOE contacts between $H_\alpha-NH_{i+2}$ of D-Trp^7 and Tyr^9 and between $NH-NH_{i+1}$ of Orn^8 and Tyr^9 indicated the presence of a β-turn. This result was supported by the observation of slowly exchanging NH resonance of residue 9 and low value of the temperature coefficient for this proton ($-\Delta\delta/\Delta T < 3.0$ ppb/K). A short stretch of antiparallel β-sheet involving residues 5−6 and 10−11 is inferred from a number of long-range NOEs including $H_\alpha-NH$ connectivities between residues 5, 11 and 10, 6 and a NH−NH connectivity between residues 6 and 9. All the data indicated the preservation, in **14** and **16**, of the β-hairpin structure.

NMR-derived constraints obtained for the analyzed peptides (Supporting Information) were used as the input data for a simulated annealing structure calculation. For each peptide, 20 calculated structures satisfying the NMR-derived constraints (violations smaller than 0.40 Å) were chosen (Figure 3a,b). As shown, both the peptides **14**, and **16** show a well-defined type II′ β-hairpin structure encompassing residue 5−10 (backbone rmsd values are 0.41 and 0.37 Å, respectively). In contrast, the N- and C-terminal residues were highly flexible. Considering the side chains orientation, Phe^6, Orn^8, and Tyr^9 side chains showed a large preference for *trans*, g^-, and g^- rotamers, respectively, while D-Trp^7 side chain is found both in *trans* and g^+ conformation.

Docking Studies of Urantide and its Analogues. The theoretical structure of the *h*-UT receptor (Figure 4) was generated by homology modeling based on the crystal structure of bovine rhodopsin (PDB code 1F88),[41] as described previously.[42] The resulting structure represents an inactive form of the *h*-UT receptor (h-UTR_i) with an overall conformation very similar to that of bovine rhodopsin (1.22 Å rmsd between the backbone atoms of the transmembrane domains).

Because the currently available docking programs may not work very well for peptide compounds, manual docking was conducted for urantide. The NMR-derived urantide structure[33] was placed in between the *trans*-membrane domains of the *h*-UTR_i, employing the following criteria to achieve meaningful docking modes: (i) The positively charged amino group of Orn^8 had to be close to and pointing in the direction of the carboxylate group of Asp130, which is conserved in many GPCRs and positioned in the TM-III region; (ii) N-terminal residues should point toward extracellular loops as experimentally determined;[43] (iii) no steric clashes should occur between any atom. To assess

Table 1. Receptor Affinity and Biological Activity of P5U and Urantide Analogues of General Formula: R-c[Pen[a]-Phe-Xaa-Yaa-Tyr-Cys]-Val-OH

peptide	Xaa	Yaa	R	pK_i[b]	pEC_{50}[c]	pK_B[d]
*h*U-II	Trp	Lys	[e]	9.10 ± 0.08	8.30 ± 0.06	
*h*U-II(4−11)	Trp	Lys	Asp	9.60 ± 0.07	8.60 ± 0.04	
P5U	Trp	Lys	Asp	9.70 ± 0.07	9.60 ± 0.07	
urantide	DTrp	Orn	Asp	8.30 ± 0.04	inactive	8.30
1	Trp	Lys	Ala	9.10 ± 0.08	8.04 ± 002	
2	DTrp	Orn	Ala	8.78 ± 0.08		7.84
3	Trp	Lys	Phe	9.55 ± 0.05	9.18 ± 0.17	
4	DTrp	Orn	Phe	7.71 ± 0.10		8.68
5	Trp	Lys	Cpa	9.05 ± 0.04	8.86 ± 0.05	
6	DTrp	Orn	Cpa	8.02 ± 0.06		7.85
7	Trp	Lys	Nal(1)	7.58 ± 0.06	6.99 ± 0.13	
8	DTrp	Orn	Nal(1)	8.41 ± 0.01		8.50
9	Trp	Lys	Nal(2)	8.19 ± 0.10	8.28 ± 0.10	
10	DTrp	Orn	Nal(2)	7.93 ± 0.01		7.89
11	Trp	Lys	(pNO_2)Phe	7.87 ± 0.08	7.14 ± 0.09	
12	DTrp	Orn	(pNO_2)Phe	7.80 ± 0.10		7.90
13	Trp	Lys	Tic	8.58 ± 0.03	8.87 ± 0.18	
14	DTrp	Orn	Tic	8.03 ± 0.07		8.94
15	Trp	Lys	Lys	8.03 ± 0.11	8.22 ± 0.24	
16	DTrp	Orn	Lys	6.66 ± 0.01		7.49

[a] Cys in *h*U-II and *h*U-II(4−11). [b] pK_i: −log K_i. [c] pEC_{50}: −log EC_{50}. [d] pK_B (−log K_B) values are from experiments in the rat thoracic aorta. Each value in the table is mean ± sem of at least four determinations. [e] H-Glu-Thr-Pro-Asp−.

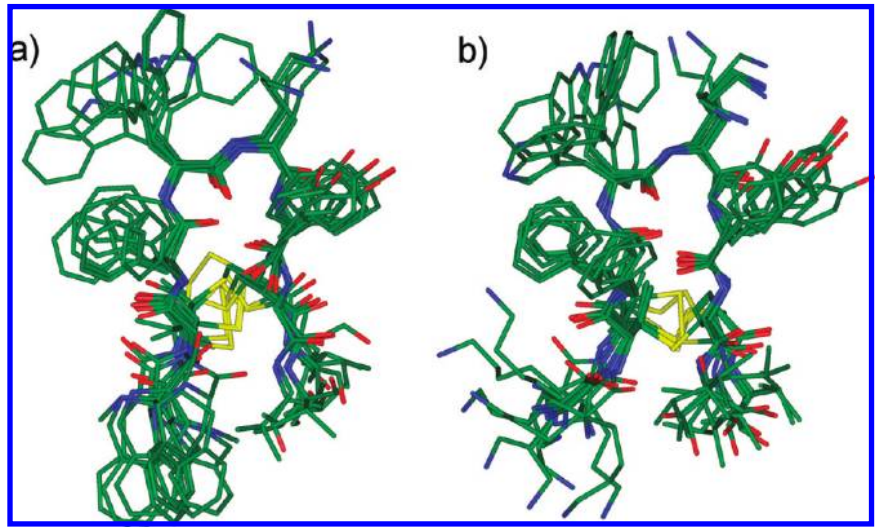

Figure 3. Superposition of the 10 lowest energy conformers of **14** (a), **16** (b). Structures were superimposed using the backbone heavy atoms of residues 5−10. Heavy atoms are shown with different colors (carbon, green; nitrogen, blue; oxygen, red; sulfur, yellow). Hydrogen atoms are not shown for clarity.

the stability of the urantide/*h*-UTR_i complex and to analyze the potential ligand/receptor interactions, energy minimization and MD simulations of 2 ns at a constant temperature of 300 K were run. During the MD simulation, the ligand, the EL's, and all the receptor side chains were allowed to relax, while the TM's and IL's backbone atoms were held frozen. The distances between the peptide and the key receptor residues were monitored along the complete 2 ns MD trajectory (Supporting Information).

To inspect the variations in the ligand conformation, rmsd with respect to the starting structure was calculated. Interestingly, the rmsd of urantide backbone atoms turned out to be remarkably stable throughout all the MD simulations (0 < rmsd <0.6), indicating that the peptide settles into the receptor-binding site in a stable β-hairpin conformation. Also the side chain orientations are those described by NMR. Interestingly, D-Trp[7] prefers a *trans* orientation about the χ_1 angle ($\chi_1 \approx 180°$, $\chi_2 \approx -70°$). As shown in Figure 5a, the hypothetical binding site of urantide is located among TM-III−TM-VII, and EL-II. The β-hairpin is oriented along the receptor helical axis, with the N- and C-terminal residues pointing toward the extracellular side. The binding mode of the peptide is determined mainly by the interactions showed in Figure 5b and Table 2.

In particular, (i) a tight charge-reinforced hydrogen-bonding network involving the carboxylate group of Asp130 and the protonated δ-amino group of Orn[8] of urantide is established. Such an interaction, which we assume to be an anchoring point of the ligand to *h*-UTR, remained stable during the whole production run (Supporting Information, Figure S2).

(ii) Three hydrophobic pockets, delimited by residues listed in Table 2, host the aromatic side chains of Phe[6], D-Trp[7], and Tyr[9] of urantide. Particularly, the indole system of D-Trp[7] appears to be optimally oriented for a π-stacking interaction with the aromatic indole system of Trp275. Furthermore, the phenolic OH of Tyr[9] is at hydrogen-bonding distance with the side chain CO of Asn297 and OH of Thr301. (iii) Asp[4] in urantide is involved in a hydrogen-bonding network. Particularly, the oxygen atoms of the carboxylate form two charge-reinforced hydrogen bonds with the Arg206 guanidinium group. In addition, the protonated N-terminal group of Asp[4] engages additional hydrogen bonds with the backbone CO of Ala187, Cys199, and Met188. (iv) Finally, the

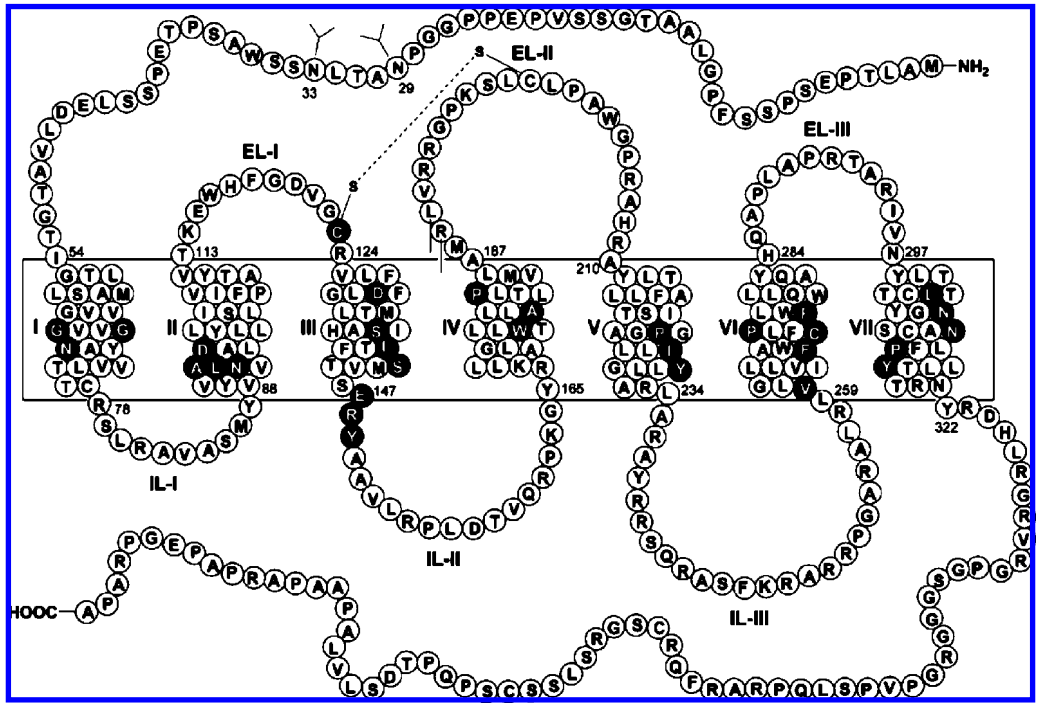

Figure 4. Serpentine model of the *h*-UTR sequence. The black lines represent the boundaries of the membrane. Filled circles indicate the residues highly conserved among the GPCRs superfamily. The TM helices are denoted by roman numerals. The arabic numbers indicate the position of the residues inside the TM domain. The glycosilation sites on the N-terminal region are also shown.

negatively charged C-terminal group establishes two hydrogen bonds with backbone HN of Cys123 and Cys 199 and a salt bridge with the protonated guanidinium moiety of Arg189 (EL-II). All the aforementioned interactions resulted to be quite stable during the whole MD production run (see Supporting Information, Figure S2−S11 for details). The mean structure of the last 1 ns of MD was extensively minimized and used for subsequent analysis.

Because the NMR results indicate that the 3D structure of the urantide analogues **14** and **16** did not change after the replacement of the N-terminal residue, we used the energy-minimized structure of the urantide/*h*-UTR$_i$ complex as a starting point for the docking procedure of these derivatives. After replacing Asp^4 of urantide with Tic^4 to give compound **14** and with Lys^4 to give **16**, the complexes were minimized and then subjected to a 200 ps MD simulation. The mean structures of the last 100 ps of the MD trajectory were then minimized and used for subsequent analysis.

While the same interactions with *h*-UTR$_i$ were recorded for the unchanged residues, in the **14**/UTR$_i$ complex, Tic^4 interacts with Val184 (TM-IV), Ala187 (EL-II), Leu200 (EL-II), Pro201 (EL-II), and Tyr211 (TM-V), while in the **16**/UTR complex Lys^4 residue takes contact with Leu200 (EL-II) and Tyr211 (TM-V). In Table 3, ligand/receptor ΔG_{bind} values are reported as calculated employing the AutoDock4 program native scoring function.[44] Interestingly, there is a clear, although qualitative, correlation between the predicted ΔG_{bind} values and the experimental binding constants (Table 1).

Docking of P5U and its Analogues. The three-dimensional model of the *h*-UTR, in the active state (*h*-UTR$_a$), was constructed from the model structure of the bovine rhodopsin, proposed by Mosberg,[45] and was generated by homology modeling following the same steps described for the inactive model.[42]

A comparison of models for the active and inactive states of *h*-UTR reveals the structural changes that accompany activation. Overall, the rmsd between these models is 2.3 Å, calculated for the backbone atoms of all the TM's, but decreases to 1.7 Å after excluding TM-VI, which experiences a rearrangements upon receptor activation. Indeed, TM-VI shifts outward and rotates counterclockwise (viewed from the extracellular side) during activation, moving its intracellular end away from TM-III and toward TM-V. As a result of this and other changes, the receptor structure tightens near its extracellular surface but opens up at the cytoplasmic side, providing a cavity for binding of the Gαs subunit.

The NMR-derived P5U structure[34] was placed in between the *trans*-membrane domains of the *h*-UTR$_a$ model, following the same criteria used for urantide (see above) to achieve meaningful binding poses. Energy minimization and MD simulations (2 ns) were run to assess the stability of the P5U/*h*-UTR$_a$ complex and to analyze the potential ligand/receptor interactions.

To inspect the variations in the ligand conformation, rmsd with respect to the starting structure was calculated. Interestingly, the rmsd of P5U backbone atoms turned out to be really stable throughout all the MD simulations ($0 < \text{rmsd} < 0.5$), indicating that the peptide settles into the receptor-binding site in a stable β-hairpin conformation. Also the side chain orientations are those described by NMR.[34]

As shown in Figure 6a, the hypothetical binding site of P5U is located among TM-III−TM-VII, EL-II, and EL-III. The β-hairpin is oriented along the receptor helical axis, with the N- and C-terminal residues pointing toward the extracellular side. The binding mode of P5U is determined mainly by the interactions showed in Figure 6b and Table 4.

As for urantide, a stable (Supporting Information, Figure S12) charge-reinforced hydrogen-bonding network involved the carboxylate group of Asp130 and the protonated ε-amino group of Lys^8 of P5U is observed. Three hydrophobic pockets, delimited by residues listed in Table 4, host the aromatic side chains of Phe^6, Trp^7, and Tyr^9. These hydro-

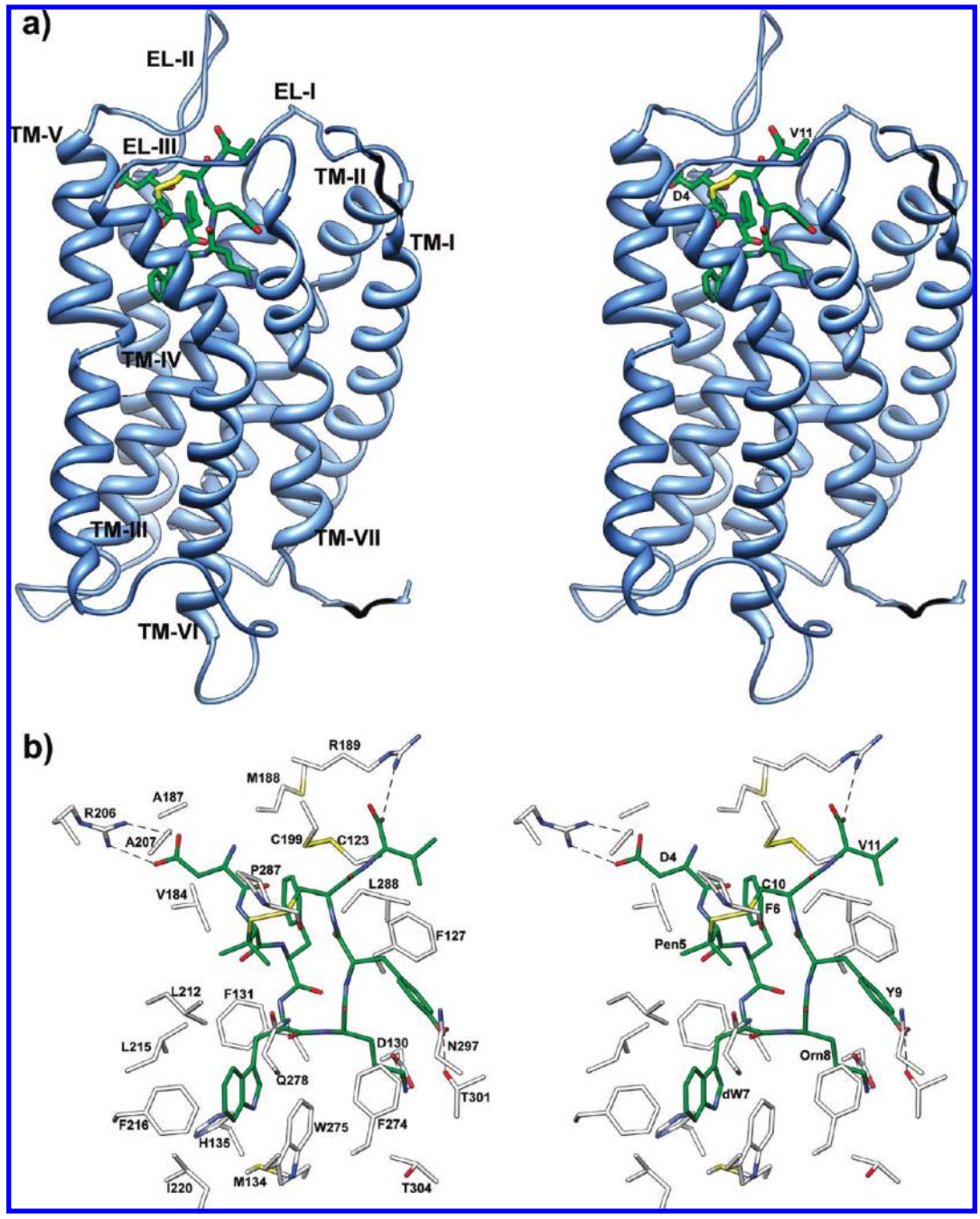

Figure 5. (a) Stereoview of *h*-UTR$_i$ model complexed with urantide. Urantide heavy atoms are color coded as in Figure 3. Receptor backbones are represented in azure and labeled. (b) Stereoview of urantide within the binding pocket of *h*-UTR$_i$. Hydrogen bonds are represented with dashed lines.

phobic pockets only partially overlap with those of urantide. For instance, Tyr^9 OH group is not engaged in any hydrogen bond. Again, the negatively charged C-terminal group of Val^{11} establishes a hydrogen bond with Cys199 backbone NH, and a salt bridge with the protonated guanidinium moiety of Arg189.

Differently from urantide, Asp^4 in P5U is involved in a hydrogen bond with the Gln285 (EL-III) NH_2 group. This H-bond is not stable during the MD trajectory (Supporting Information, Figure S13). The mean structure of the last 1 ns of MD was extensively minimized and used for subsequent analysis.

Replacing the Asp^4 residue of P5U with Tic or Lys residue (obtaining the derivatives **13** and **15**, respectively) in the P5U/*h*-UTR model complex, and following the same optimization steps used for the complexes of urantide analogues (see above), we obtained the two models: **13**/*h*-UTR$_a$ and **15**/*h*-UTR$_a$, showing similar binding energy (Table 3) in accordance with the experimental binding data (Table 1).

Switching the Ligands. To assess the predictive value of the receptor models, the ligands were switched, i.e., urantide was docked within *h*-UTR$_a$ and P5U within *h*-UTR$_i$ model (Supporting Information, Figure S14). For the docking of urantide, we started from the optimized P5U/UTR$_a$ complex and superposed the NMR derived urantide structure with that of P5U (backbone atoms of residues 5−10). Then, we removed the P5U structure and optimized the urantide/UTR$_a$ complex. Analogous

Table 2. Urantide/*h*-UTR$_i$ Interactions

residue[a]	surrounding residue
Asp^4	Ala187 (EL-II), Met188 (EL-II), Cys199 (EL-II), Arg206 (EL-II), Ala207 (EL-II)
Pen^5	Gln278 (TM-VI), Pro287 (EL-III)
Phe^6	Cys123 (EL-I), Val184 (TM-IV), Met188 (EL-II)
D-Trp^7	Phe131 (TM-III), Met134 (TM-III), His135 (TM-III), Leu212 (TM-V), Leu215 (TM-V), Phe216 (TM-V), Ile220 (TM-V), Trp275 (TM-VI), Gln278 (TM-VI)
Orn^8	Asp130 (TM-III), Thr301 (TM-VII), Thr304 (TM-VII)
Tyr^9	Phe127 (TM-III), Phe274 (TM-VI), Asn297 (TM-VII), Thr301 (TM-VII)
Cys^{10}	Cys199 (EL-II), Pro287 ((EL-III)
Val^{11}	Cys123 (EL-I), Arg189 (EL-II), Cys199 (EL-II), Leu288 (EL-III).

[a] For sake of clarity, the residue numbers of the ligands are reported as apex while those of the receptor are not.

Table 3. Binding Free Energies (ΔG_{AD4}) Calculated for the Energy Minimized Averaged Complexes Deriving from the MD Simulations

receptor	ligand	ΔG_{bind}[a]	electr[b]	H-bond[b]	VdW[b]	desolv[b]	tors[b]
h-UTR$_i$[c]	urantide	−24.33	−4.99	−5.90	−26.50	7.09	5.97
h-UTR$_i$	**14**	−23.01	−3.21	−3.83	−26.98	5.94	5.07
h-UTR$_i$	**16**	−21.10	−3.31	−5.77	−25.16	6.28	6.86
h-UTR$_a$	P5U	−24.53	−4.99	−6.11	−25.89	6.69	5.76
h-UTR$_a$	**13**	−23.53	−3.35	−4.19	−27.40	6.03	5.37
h-UTR$_a$	**15**	−23.01	−4.11	−6.77	−25.40	6.31	6.96
h-UTR$_a$	urantide	−20.65	−5.92	−6.42	−21.39	7.11	5.97
h-UTR$_i$	P5U	−18.68	−3.60	−3.47	−24.67	6.80	6.26

[a] ΔG_{bind}: free energy of binding. [b] Energy terms contributing to the AutoDock4 scoring function. electr: electrostatic; H-bond: H-bonding; VdW: van der Waals; desolv: desolvation; tors: torsional entropy. All terms are given in kcal/mol. [c] *h*-UTR$_i$: receptor in the inactive state. *h*-UTR$_a$: receptor in the active state.

steps were taken for the P5U/UTR$_i$ complex. In Table 3, the binding energies of the two complexes are reported.

Discussion

Previous studies have demonstrated that the C-terminal octapeptide of *h*U-II [U-II(4−11), Table 1] mimicked the effects of U-II on intracellular calcium concentration in UTR-transfected cells and contraction of rat aortic rings.[22,24,25] Recently, Coy et coll. have examined the role of the N-terminal Asp residue in UII(4−11) because this acidic amino acid embodies one of the main structural differences between the UII(4−11) and somatostatin octapeptides, which results in little somatostatin affinity for the UT receptor.[26] They found that the N-terminal amino acid does not require a negatively charged side chain, merely one which has a hydrogen bond acceptor CO group. The side chain can be constrained into a *trans*-olefinic configuration and can also contain an aromatic ring substituted with polar groups such as OH and NO_2. Afterward, Salvadori et coll. examined the same position of *h*U-II(4−11) using a number of aromatic residues.[46] They found that all of the new analogues behaved as full agonists and that aromaticity is well tolerated; size, length, and chirality of the side chain are not important, while substituents with a nitrogen atom are preferred. On bases of these considerations and to further investigate the contribution of the N-terminal Asp residue in the biological activity, we synthesized 16 analogues of P5U and urantide substituted at this position with amino acids bearing different physicochemical properties (Table 1). In particular, urantide was used as lead compound to investigate the N-terminal position in analogues with potential antagonist activity. All synthesized compounds were tested for their binding affinity on *h*-UTR-transfected CHO cells and for their contractile activity on de-endothelialized rat aortic rings (Table 1).[31]

Overall, the biological data indicate that in the "agonist series" (i.e., derived from P5U), the N-terminal substitutions of Asp^4 with uncharged, aromatic, or positively charged residues are generally well tolerated. The consistent reduction in binding and activity is probably due to the lost of a hydrogen bond acceptor/donor group, in accordance with previous results.[26,46] Concerning the "antagonist series" (i.e., derived from urantide), while a positively charged amino acid (Lys) strongly reduces the binding and the activity (compound **16**), an aromatic residue is well tolerated and can increase the potency. In particular, compound **14**, in which a Tic residue replaces the Asp^4 of urantide, showed the highest antagonist potency in the functional rat aorta bioassay (pK_B 8.94). Because the binding constant of **14** to *h*-UTR is slightly reduced compared to urantide, the enhanced functional potency should derive from improved tissue penetration of the more hydrophobic Tic amino acid in **14** replacing an Asp residue in urantide. Species differences between *h*-UTR and *r*-UTR could also be invoked. To check the last hypothesis, the sequences of *h*-UTR and *r*-UTR were compared (Supporting Information, Figure S15). Because only minimal residue differences were observed near the bound ligand and, in particular, near to the Tic residue (EL2 is unchanged in the two receptors), the hypothesis was rejected.

To determine whether the different biological activities of urantide analogues were driven by different conformational properties of the peptides or by the different chemical functionalities at the N-terminus, we performed an NMR study on the interesting analogues **14** and **16** in SDS micelles solution. The use of SDS micelles to study the conformational properties of *h*U-II analogues is motivated on the basis of their interaction with a membrane receptor. For peptides acting as ligands of membrane receptors (such as GPCR), the use of membrane mimetic media is suggested, hypothesizing a membrane-assisted mechanism of interactions between the peptides and their receptors.[47] According to this model, the membrane surface plays a key role in facilitating the transition of the peptide from a random coil conformation adopted in the extracellular environment to a conformation that is recognized by the receptor. The increase of the local concentration of the peptide and the reduction of the rotational and translational freedom of the neuropeptide are membrane-mediated events acting as determinant steps for the conformational transition of the peptide.[48] Actually, we succeeded in correlating the SDS-bound conformation of *h*U-II analogues with their biological activity.[33,34]

We showed that *h*U-II analogues, which retain high affinity for UT receptor, all possess a type II′ β-hairpin backbone conformation regardless their agonist or antagonist activity, indicating that such backbone conformation is necessary for the UT recognition.[33,34] The main conformational difference observed in the structures of the antagonists and the agonists was established in a different orientation of the (D/L)-Trp^7 side chain. In particular, while in the agonists the (D/L)-Trp^7 indole moiety is close to the Lys^8 side chain, in the antagonists (D/L)-Trp^7 side chain is more flexible and further from the ornithine side chain. The structural features of the "antagonist series" were found also for the analogues **14** and **16** (Figure 3), indicating that the different affinity-activity of the two compounds does not depend on a different spatial disposition of the "pharmacophoric" residues (i.e., (D/L)-Trp^7, Lys/Orn^8, Tyr^9)[22,23] but must depend on different interaction of the N-terminal residue with the receptor.

To gain insight into this interaction mode we first undertook a docking study between the parent urantide and *h*-UT receptor model. It is worth noting that, while docking studies regarding

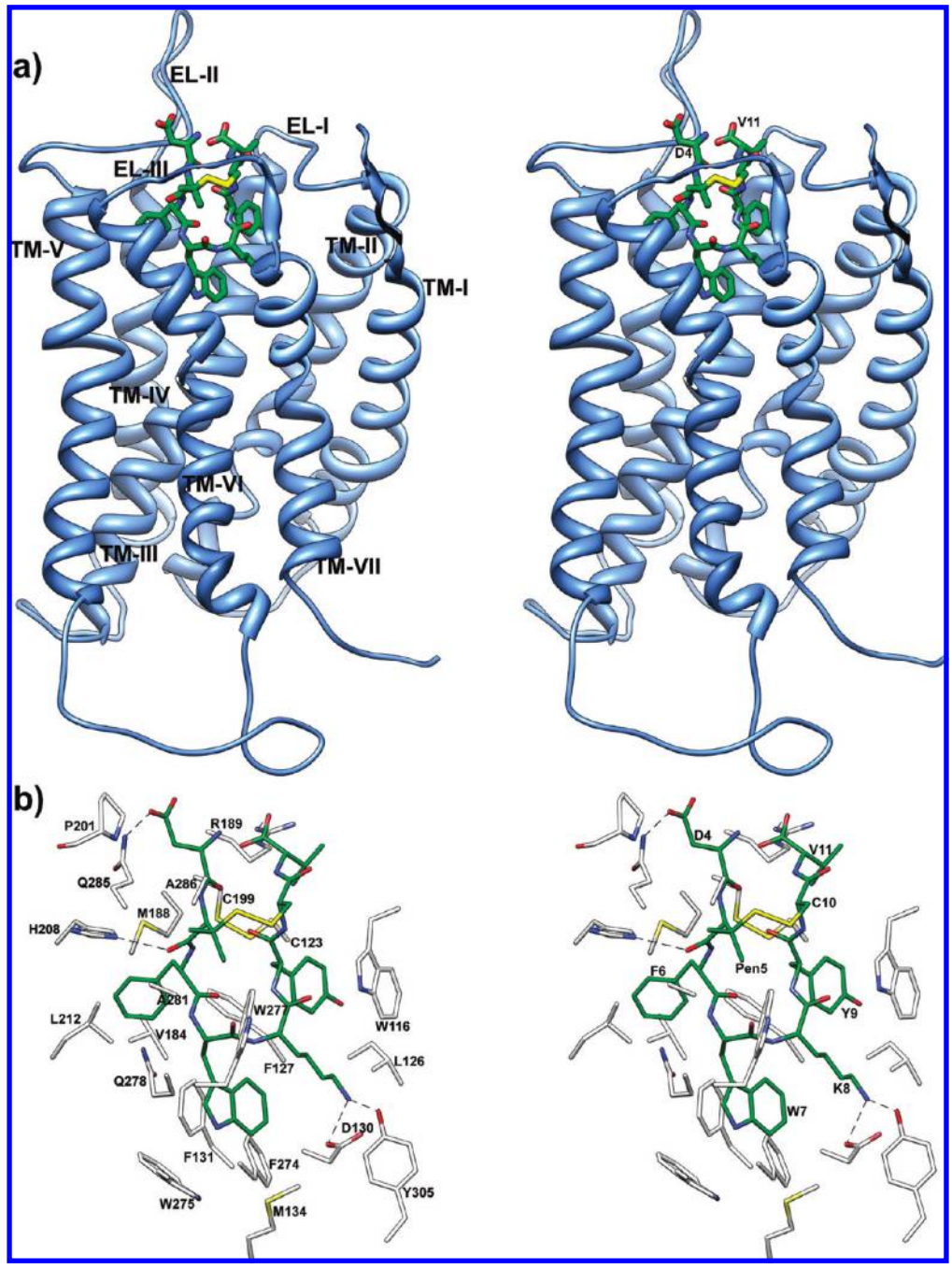

Figure 6. (a) Stereoview of *h*-UTR$_a$ model complexed with P5U. P5U heavy atoms are color coded as in Figure 3. Receptor backbones are represented in azure and labeled. (b) Stereoview of P5U within the binding pocket of *h*-UTR$_a$. Hydrogen bonds are represented with dashed lines.

Table 4. P5U/*h*-UTR$_a$ Interactions

residue	surrounding residue
Asp[4]	Pro201 (EL-II), Gln285 (EL-III)
Pen[5]	His208 (EL-II), Trp277 (TM-VI), Ala281 (TM-VI), Ala286 (EL-III)
Phe[6]	Val184 (TM-IV), Met188 (EL-II), Leu212 (TM-V)
Trp[7]	Phe131 (TM-III), Met134 (TM-III), Phe274 (TM-VI), Trp275 (TM-VI), Gln278 (TM-VI)
Lys[8]	Asp130 (TM-III), Tyr305 (TM-VII)
Tyr[9]	Trp116(TM-II), Cys123 (EL-I), Leu126 (TM-III), Phe127 (TM-III), Cys199 (EL-II)
Cys[10]	Trp277 (TM-VI)
Val[11]	Arg189 (EL-II), Cys199 (EL-II)

peptide agonists have been performed,[23,42,43,49] the docking of a peptide antagonist at the UT receptor is unprecedented. Because the crystal structure of a GPCR in the active conformation is not yet disposable, we used the "active state" rhodopsin model developed by Mosberg et al. as a template to build an *h*-UTR$_a$ model.[45] Hence, the rhodopsin receptor template was also chosen for the inactive state model (*h*-UTR$_i$) to allow a direct comparison of the two models. The structures of other mammalian GPCR's in inactive state have been solved.[50−52] Interestingly, our *h*-UTR$_i$ model and the β_2-adrenergic receptor (β_2AR, PDB code 2RH1) are quite similar around the urantide binding site, showing an rmsd of the backbone heavy atoms of 1.5 Å (helices II−VII, Supporting Information, Figure S16).

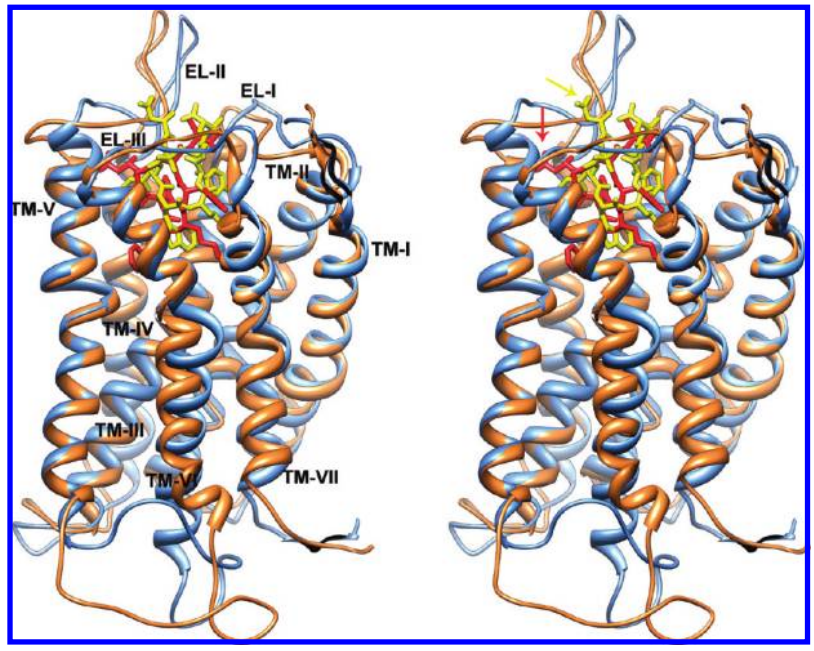

Figure 7. (a) Stereoview of *h*-UTR models in the inactive (azure) and active (sienna) conformations complexed with urantide (red) and P5U (gold), respectively. The *h*-UTR models are superimposed using the backbone heavy atoms of TM residues apart from TM-VI. Asp^4 residue is evidenced by an arrow.

Urantide/*h*-UTR_i complex (Figure 5) and the MD simulations indicated that: (i) the β-hairpin structure adequately fits the binding site and is stable during the MD trajectory, (ii) the binding site, situated in the entrance of the TM bundle on the extracellular side, is formed by TM-III−TM-VII, and EL-II, (iii) particularly important for the present study, the N-terminal Asp^4 residue interacts with EL-II, mostly by stable electrostatic interactions, with the Arg206. Replacement of Asp^4 with a Lys residue (analogue **16**) in the model complex increases the binding energy (Table 3) because the favorable interactions are lost and, in contrast, electrostatic repulsions between N^{ε} of Lys^4 and the guanidinium group of five arginine and the N^{ε} of one lysine residues located on the EL-II can occur. In contrast, the loss of favorable electrostatic interaction, upon the replacement of the Asp^4 of urantide with a Tic residue (analogue **14**), is partially compensated by van der Waals interactions of the phenyl ring of Tic and by a reduced desolvation energy.

Docking study between P5U and *h*-UTR_a was also performed. The obtained complex (Figure 6) and the MD simulations indicated that: (i) the β-hairpin structure adequately fits the binding site and is stable during the MD trajectory, (ii) the binding site, situated in the entrance of the TM bundle on the extracellular side, is formed by TM-III−TM-VII, EL-II, and EL-III, (iii) the N-terminal Asp^4 residue lies between EL-II and EL-III. We found similarities, but also some differences, with previous reports describing the docking of peptide agonists (*h*U-II and P5U) into an UTR model.[23,42,43,49] With regard to our previous work,[42] the different docking results obtained for the P5U/*h*-UTR complex is ascribable to the different conformation of both the receptor and the ligand. In fact, in the present study, the *h*-UTR structure is based on an active model of rhodopsin,[45] while in the previous work the receptor was constructed starting from the X-ray inactivated form of rhodopsin.[41] Moreover, herein the presented P5U 3D structure is obtained from a NMR study in SDS micelle solution,[34] while the one used in 2005 was derived from a NMR study in DMSO solution.[30]

To assess the predictive value of the models the ligands were switched, i.e., urantide was docked within *h*-UTR_a model and P5U within *h*-UTR_i (Supporting Information, Figure S14). Both urantide/UTR_a and P5U/UTR_i complexes show negative binding energies (Table 3), but these are significantly lower (absolute value) than the ones of urantide/UTR_i and P5U/UTR_a complexes, respectively. These results are not surprising. In fact, urantide still retains agonist activity, being a full agonist in a calcium mobilization assay.[32] Interestingly, D-Trp^7 aromatic moiety of urantide within UTR_a binding site is close to the Orn^8 side chain in a conformation which characterizes the agonist peptide ligands (Supporting Information, Figure S14).[33] As concern P5U/UTR_i complex, the negative value of the binding energy can be explained by admitting that, in a first step, even the agonists bind the receptor in its inactive (ground) state. Then, the system moves to a minimum of free energy, which is reached with the receptor activation.

Urantide/*h*-UTR_i and P5U/*h*-UTR_a interactions found in our models (Tables 2, 4 and Figure 7) are different. In particular, urantide plunges more deeply into the TM's bundle compared to P5U, probably due to the ornithine side chain length reduction, and to the D-Trp^7 higher flexibility. As a consequence, the exocyclic carboxylate group of Asp^4 of P5U, lying at the interface between EL-II and EL-III, is more external compared to the that of the corresponding residue in urantide and establishes only nonstable hydrogen bond with the receptor. In accordance with SAR data obtained by us and others,[26,46] the presence of both aromatic (**13**) or positively charged (**15**) residues at position 4 of P5U leads to compounds with similar binding energy (Table 3).

Recently published experimental results, reporting that the agonists and antagonists (partial agonists) interact differently with the UT receptor are, in accordance with our models.[43,53] Boivin et al. measured the interactions of *h*U-II, URP, and urantide with separately synthesized *h*-UT receptor EL's.[53,54] They observed that agonist *h*U-II and URP bind EL-II and EL-III while the binding of urantide was observed only with EL-II. None of these ligands were able to interact with EL-I. These

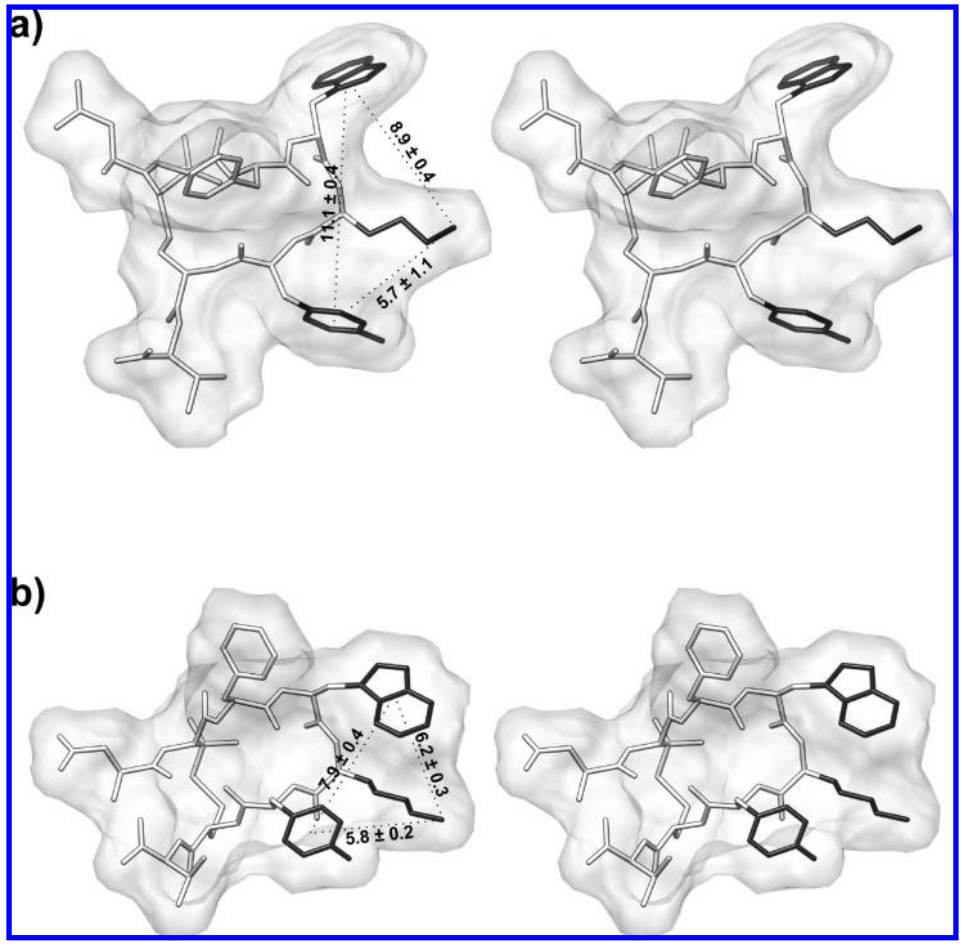

Figure 8. Stereoview of the pharmacophore model for peptide antagonists (a) and agonists (b). The distances between the aryl ring centroids of (D)Trp[7] and Tyr[9] and the $N^{\varepsilon/\delta}$ of Lys(Orn)[8] are displayed. Distances and standard deviations are obtained from 100 structures saved every 20 ps of the MD simulations.

results are fully consistent with our models. Leduc et al. found various interactions between photoreactive *h*U-II and urantide analogues and *r*-UTR.[43,55] Also, these interactions are compatible with our models.

The proposed binding modes are also in qualitative agreement to the observed SAR at the core -Phe-Trp-Lys-Tyr- sequence. In fact, pharmacophoric residues Trp[7], Lys(Orn)[8], and Tyr[9], whose substitution with Ala significantly reduces or abolishes the binding affinity of U-II analogues, show a high number of receptor interactions. In contrast, Phe[6] shows only a few interactions in accordance with SAR indicating that its substitution with Ala results in a still full agonist peptide. Furthermore, substitution of the hydroxyl group of Tyr[9] of U-II with methoxy, nitro, amino, methyl, fluoro, or a hydrogen atom does not affect the potency and the efficacy of the U-II analogues in the rat aorta bioassay.[56] These observations agree with our model because the phenolic OH is not involved in receptor binding in the P5U/UTR_a model. Substitution of the Tyr residue by bulky aromatic amino acids such as (2-naphthyl)-L-alanine, biphenylalanine[23] or 3-iodo-tyrosine[25] may even increase the binding affinity and the biological activity. Consistently, the tyrosine-binding pocket of our model can accommodate a bulkier side chain with an enhancement of the hydrophobic interactions. SAR data suggest that the presence of an aliphatic amine at position 8 is mandatory for U-II activity.[56] The position of the NH_2^{ε} from the peptide backbone has been investigated using ornithine, 2,4-diaminobutyric acid (Dab), and 2,3-diaminopropionic acid (Dap), i.e., with distances of 3, 2, and 1 carbon atoms, respectively. Reduction of the distance between the primary aliphatic amine and the peptide backbone of 3 and 2 methylene groups gradually reduces the potency and efficacy of the analogues and switch the activity toward antagonism. Further shortening of the amino acid side-chain increases potency and restores efficacy. Interestingly, the Dab[8]-urantide analogue UFP-803 behaves as a pure antagonist (pA_2 7.46).[57] Our model can explain these results. In fact, a distance of 3 methylene groups is suitable for both UTR_i and UTR_a ligands, such as urantide ($\Delta\Delta G_{bind} = -3.88$ kcal/mol, Table 3). A distance of 2 methylene groups is also suitable for the two receptor states but with a much preferred antagonist mode (for UFP-803, $\Delta\Delta G_{bind} = -5.41$ kcal/mol; data not shown). Little attention has been paid to the Trp[9] residue in the SAR studies of U-II apart from the Ala- and D-scan approaches. Replacement of the Trp residue with 2-Nal[23] or 4-benzoyl-L-phenylalanine (Bpa)[55] significantly decreased agonist binding affinity and potency. This would suggest that the indole NH function may establish a hydrogen bond with some UTR residue. We do not observe this postulated H-bond and believe that the indole electron rich system is more suitable for a cation$-\pi$ interaction with the Lys[8] side chain observed in the peptide agonist ligands.[33]

On the basis of the binding mode of UTR peptide agonists and antagonists, we derived new 3D pharmacophore models illustrated in Figure 8. The distances between the pharmacophoric residues (i.e., mean distances observed during the 2 ns MD simulations) are in good accordance with those previously reported both for peptide agonists and antagonists.[33] These

pharmacophore models might be useful for the next design cycle and, in particular, for the design of small-molecule ligands.

Conclusions

In conclusion, we observed a different SAR at the N-terminus for P5U compared to urantide analogues. P5U shows a high degree of tolerance upon N-terminal substitutions. In urantide analogues, an aromatic residue is well tolerated and can increase the potency. In fact, replacement of the Asp[4] residue by Tic led to an analogue, compound **14**, more potent as an antagonist ($pK_B = 8.94$) compared to urantide. Conversely, a positively charged amino acid (Lys) drastically reduces the binding and the activity. The results could be explained on the basis of the different receptor binding mode of the agonist P5U vs the antagonist urantide. Understanding of the impact of amino acid substitutions in position 4, combined with information regarding the interactions between UT receptor and its ligands, is crucial to increase the knowledge of structure−function relationships focused to the design of new potent UT receptor ligands.

Experimental Section

Synthesis. N^{α}-Fmoc-protected amino acids, HBTU and HOBt, were purchased from Inbios (Naples, Italy). Wang resin was purchased from Advanced ChemTech (Louisville, KY). Protected Pen was purchased from Bachem (Basel, Switzerland). Peptide synthesis solvents, reagents, as well as CH_3CN for HPLC were reagent grade and were acquired from commercial sources and used without further purification unless otherwise noted. The synthesis of *h*U-II analogues was performed in a stepwise fashion via the solid-phase method. N^{α}-Fmoc-Val-OH was coupled to Wang resin (0.5 g, 0.7 mmol NH_2/g). The following protected amino acids were then added stepwise N^{α}-Fmoc-Cys(Trt)-OH, N^{α}-Fmoc-Tyr(OtBu)-OH, N^{α} -Fmoc-Yaa(N^{ε}-Boc)-OH (Yaa: Lys, Orn), N^{α}-Fmoc-Xaa(N^{in}-Boc)-OH (Xaa: Trp, DTrp), N^{α}-Fmoc-Phe-OH, N^{α}-Fmoc-Pen(Trt)-OH, and N^{α}-Fmoc-R-OH (R = Phe, Cpa, Ala, (pNO_2)Phe, Tic, Nal(1), Nal(2), Lys). Each coupling reaction was accomplished using a 3-fold excess of amino acid with HBTU and HOBt in the presence of DIEA.

The N^{α}-Fmoc protecting groups were removed by treating the protected peptide resin with a 25% solution of piperidine in DMF, (1 × 5 min and 1 × 20 min). The peptide resin was washed three times with DMF, and the next coupling step was initiated in a stepwise manner. All reactions were performed under an Ar atmosphere. The peptide resin was washed with DCM (3×), DMF (3×), and DCM (4×), and the deprotection protocol was repeated after each coupling step. The N-terminal Fmoc group was removed as described above, and the peptide was released from the resin with TFA/ Et_3SiH /H_2O (90:5:5) for 3 h. The resin was removed by filtration, and the crude peptide was recovered by precipitation with cold anhydrous ethyl ether to give a white powder, which was purified by RP-HPLC on a semipreparative C18-bonded silica column (Vydac 218TP1010, 1.0 cm × 25 cm) using a gradient of CH_3CN in 0.1% aqueous TFA (from 10 to 90% in 45 min) at a flow rate of 1.0 mL/min. The product was obtained by lyophilization of the appropriate fractions after removal of the CH_3CN by rotary evaporation. Analytical RP-HPLC indicated a purity >98%, and molecular weights were confirmed by FAB-MS (Fisons model Prospec) or HR-MS (Kratos Analytical model Kompact) (Supporting Information).

General Method of Oxidation and Cyclization. The peptides were oxidized by the syringe pump method previously reported.[58] The linear peptide (300−500 mg) was dissolved in 40 mL of 50%H_2O/25% acetonitrile/25% methanol, and nitrogen gas was passed through the solution for 20 min. Then 5 mL of saturated ammonium acetate solution were added, and the pH was taken to 8,5 with NH_4OH. The peptide solution was then added at room temperature via syringe pump to a stirred oxidant solution. The oxidant solution was prepared as follows: 2 equiv of potassium ferricyanide were dissolved in 400 mL of H_2O/200 mL of acetonitrile/200 mL of methanol. To this solution was added 100 mL of saturated ammonium acetate, and the pH was then taken to 8.5 with NH_4OH. The peptide solution was added at such a rate that approximately 10 mg of peptide were delivered per hour per liter of the oxidant. After the addition of peptide was complete, the reaction mixture was stirred for an additional 5−6 h and then taken to pH 3.5 with glacial acetic acid. Amberlite IRA-68 (Cl form) was added to remove the iron ions and the solution stirred for 20 min and then filtered. The solution was concentrated using a rotary evaporator at 30 °C and then lyophilized. The material thus obtained was dissolved in glacial acetic acid, filtered to remove inorganic salts, and relyophilized. The crude cyclic peptides were purified by preparative HPLC on the system described above, using a gradient of 100% buffer for 20 min, then 0−20% acetonitrile in 5 min, followed by 20−60% acetonitrile in 40 min, all at 40 mL/min. Again the peptides eluted near 50% organic/50% buffer. The purity of the cyclic peptides was checked by analytical HPLC (C-18 column, Vydac 218TP104, 4.6 mm × 25 cm), using a Shimadzu SPD 10A vp with detection at 230 and 254 nm and by TLC in four solvent systems in silica gel with detection by UV light, iodine vapors, and ninhydrin. The analytical data of the compounds synthesized in this paper are given in the Supporting Information.

Organ Bath Experiments. The experimental procedures employed in this study were approved by Institutional Animal Care and Use Committee and carried out in accordance with the legislation of Italian authorities (D.L. 116 27/01/1992), which complies with European Community guidelines (CEE Directive 86/609) for the care and use of experimental animals.

Male albino rats (Wistar strain, 275−350 g) were euthanized by cervical dislocation under ether anesthesia. The thoracic aorta was cleared of surrounding tissue and excised from the aortic arch to the diaphragm. From each vessel, a helically cut strip was prepared and then it was cut into two parallel strips. The endothelium was removed by gently rubbing the vessel intimal surface with a cotton-tip applicator; the effectiveness of this maneuver was assessed by the loss of relaxation response to acetylcholine (1 μM) in noradrenaline (1 μM) precontracted preparations. All preparations were placed in 5 mL organ baths filled with normal Krebs solution warmed at 37 °C and oxygenated with 95% O_2, 5% CO_2. The tissues were connected to isotonic force transducers (Ugo Basile, VA, Italy) under a constant load of 5 mN, and motor activity was digitally recorded by an Octal bridge amplifier connected to PowerLab/8sp hardware system and analyzed using the Chart 4.2 software (AD Instruments, Australia). After 60 min of equilibration, tissue responsiveness was assessed by the addition of 1 μM noradrenaline followed by a further equilibration of 60 min.

To assess the agonist activity cumulative concentration−response curves to *h*U-II and to the agonist peptide under examination were constructed in paired aortic strips, and responses obtained were normalized toward the control *h*U-II maximal contractile effect (E_{max}).

To assess the antagonist activity concentration−response curves to *h*U-II were constructed cumulatively in paired aortic strips. One strip was pretreated with vehicle (DMSO; 1−3 μL/mL) and used as a control, while the other strip was pretreated with the antagonist peptide under examination and, after a 30 min incubation period, *h*U-II was administered cumulatively to both preparations.

In each preparation, only one cumulative concentration−response curve to *h*U-II was carried out and only one concentration of antagonist was tested. Concentration−response curves were analyzed by sigmoidal nonlinear regression fit using the GraphPad Prism 4.0 program (San Diego, CA) to determine the molar concentration of the agonist producing the 50% (EC_{50}) of its maximal effect. Agonist activity of all compounds was expressed as pEC_{50} ($-\log EC_{50}$). The antagonist potency was expressed as apparent pK_B ($-\log K_B$) calculated from the equation: $pK_B = -(\log [CR - 1] - \log [\text{antagonist concentration}])$, where the concentration ratio (CR) is the ratio of equieffective concentrations (EC_{50}) of hU-II in the presence and absence of antagonist.[59] The nature of the antagonism was checked by means of Schild analysis.

Binding Experiments. All experiments were performed on membranes obtained from stable CHO-K1 cells expressing the recombinant human UT receptor (Euroscreen ES-440-M, Bruxelles, Belgium). Assay conditions were: TRIS-buffer (20 mM, pH 7.4 at 37 °C) added with $MgCl_2$ (5 mM) and 0.5% BSA. Final assay volume was 0.1 mL, containing 1 μg membrane proteins. The radioligand used for competition experiments was [^{125}I]urotensin II (specific activity 2000 Ci/mmol; Amersham Biosciences, Buckinghamshire, U.K.) in the range 0.07−1.4 nM (corresponding to 1/10−1/5 of its KD). Nonspecific binding was determined in the presence of 1 μM of unlabeled *h*U-II and ranged between 10−20% of total binding. Competing ligands were tested in a wide range of concentrations (1 pM−10 μM). The incubation period (120 min at 37 °C) was terminated by rapid filtration through UniFilter-96 plates (Packard Instrument Company), presoaked for at least 2 h in BSA 0.5%, and using a MicroMate 96 cell harvester (Packard Instrument Company). The filters were then washed 4 times with 0.2 mL aliquots of Tris-HCl buffer (20 mM, pH 7.4, 4 °C). Filters were dried and soaked in Microscint 40 (50 μL in each well, Packard Instrument Company), and bound radioactivity was counted by a TopCount microplate scintillation counter (Packard Instrument Company). Determinations were performed in duplicate. All binding data were fitted by using GraphPad Prism 4.0 in order to determine the equilibrium dissociation constant (K_d) from homologous competition experiments, the ligand concentration inhibiting the radioligand binding of the 50% (IC_{50}) from heterologous competition experiments. K_i values were calculated from IC_{50} using the Cheng−Prusoff equation ($K_i = IC_{50}/(1 + [\text{radioligand}]/K_d)$) according to the concentration and K_d of the radioligand.[49]

NMR Sample Preparation. ^2H_2O (99.9%) was obtained from Aldrich (Milwaukee, WI), 98% SDS-d_{25} was obtained from Cambridge Isotope Laboratories, Inc. (Andover, MA), and [(2,2,3,3-tetradeuterio-3-(trimethylsilanyl)]propionic acid (TSP) from MSD Isotopes (Montreal, Canada).

NMR Spectroscopy. The samples for NMR spectroscopy were prepared by dissolving the appropriate amount of peptide in 0.45 mL of ^1H_2O (pH 5.5), 0.05 mL of ^2H_2O to obtain a concentration 1−2 mM of peptides and 200 mM of SDS-d_{25}. NH exchange studies were performed dissolving peptides in 0.50 mL of ^2H_2O and 200 mM of SDS-d_{25}. NMR spectra were recorded on a Varian INOVA 700 MHz spectrometer equipped with a *z*-gradient 5 mm triple-resonance probe head. All the spectra were recorded at a temperature of 25 °C. The spectra were calibrated relative to TSP (0.00 ppm) as internal standard. One-dimensional (1D) NMR spectra were recorded in the Fourier mode with quadrature detection. The water signal was suppressed by gradient echo.[60] 2D DQF-COSY,[37] TOCSY,[38] NOESY,[39] and PE-COSY[61] spectra were recorded in the phase-sensitive mode using the method from States.[62] Data block sizes were 2048 addresses in t_2 and 512 equidistant t_1 values. Before Fourier transformation, the time domain data matrices were multiplied by shifted $\sin^2$ functions in both dimensions. A mixing time of 70 ms was used for the TOCSY experiments. NOESY experiments were run with mixing times in the range of 150−300 ms. The qualitative and quantitative analyses of DQF-COSY, TOCSY, and NOESY spectra were obtained using the interactive program package XEASY.[40] $^3J_{HN-H\alpha}$ coupling constants were obtained from 1D ^{1}H NMR and 2D DQF-COSY spectra. $^3J_{H\alpha-H\beta}$ coupling constants were obtained from 1D ^{1}H NMR and 2D PE-COSY spectra, the last performed with a β flip angle of 35°. The temperature coefficients of the amide proton chemical shifts were calculated from 1D ^{1}H NMR and 2D TOCSY experiments performed at different temperatures in the range 25−40 °C by means of linear regression.

Structural Determinations. The NOE-based distance restraints were obtained from NOESY spectra collected with a mixing time of 200 ms. The NOE cross peaks were integrated with the XEASY program and were converted into upper distance bounds using the CALIBA program incorporated into the program package DYANA.[63] Cross peaks, which were overlapped more than 50%, were treated as weak restraints in the DYANA calculation. In a first step, only NOE derived constraints (Supporting Information) were considered in the annealing procedures. Overall, 76 meaningful NOE-derived restraints (9 NOEs per residue; that is: 32 intraresidue, 32 sequential, 11 medium-range, and 1 long-range) for peptide **14**, and 73 (9 NOEs per residue; that is: 34 intraresidue, 29 sequential, 9 medium-range, and 1 long-range) for peptide **16**, were used as input for the calculation. For each examined peptide, an ensemble of 200 structures was generated with the simulated annealing of the program DYANA. An error-tolerant target function (tf-type = 3) was used to account for the peptide intrinsic flexibility. Nonstandard Pen, D-Trp, Orn, and Tic residues were added to DYANA residue library using MOLMOL.[64] From these structures, we could univocally determine the hydrogen bond atom acceptors corresponding to the slowly exchanging NH's previously determined for each peptide. In a second DYANA run, these hydrogen bonds were explicitly added as upper and lower limit constraints (NH of Phe^6 with CO of Tyr^9, and NH of Tyr^9 with CO of Phe^6), together with the NOE derived upper limit constraints (Supporting Information). The second annealing procedure produced 200 conformations from which 50 structures were chosen, whose interprotonic distances best fitted NOE derived distances, and then refined through successive steps of restrained and unrestrained EM calculations using the Discover algorithm (Accelrys, San Diego, CA) and the consistent valence force field (CVFF)[65] as previously described.[34] Coupling constants were not used in the constrained simulated annealing calculation, however, backbone and side chain conformations are in accordance with the experimental $^3J_{HN-H\alpha}$ and $^3J_{H\alpha-H\beta}$ coupling constants, respectively. The final structures were analyzed using the InsightII program (Accelrys, San Diego, CA). Graphical representation were carried out with the InsightII program (Accelrys, San Diego, CA). rms deviation analysis between energy minimized structures were carried out with the program MOLMOL.[64]

***h*-UTR Models and Docking.** The theoretical structure of the *h*-UT receptor, in the inactive state, was generated by homology modeling based on the crystal structure of bovine rhodopsin (PDB code 1F88),[41] as previously described.[42] The three-dimensional model of the *h*-UTR, in the active state, was constructed from the model structure of the bovine rhodopsin, proposed by Mosberg,[45] and was generated by homology modeling following the same steps described for the inactive model.[42] To validate the reliability of the calculated models, the program PROCHECK,[66] which automatically checks the stereochemical accuracy, packing quality, and folding reliability, was employed. All amino acids in the α-helices were located in the favored region of the right-handed α-helix in the Ramachandran plot. From calculated ω angles, there were no *cis* peptide bonds in the calculated *h*-UTR model. All Cα atoms except Cys displayed *S*-chirality. For the packing quality, there were no bump regions in the calculated *h*-UTR models.

The peptides urantide and P5U were manually docked in the suspected binding site of the *h*-UTR$_i$ and *h*-UTR$_a$, respectively. Employing the criteria described in the Results section, we generated 10 poses for both urantide/*h*-UTR$_i$ and P5U/*h*-UTR$_a$ complexes. Refinement of each pose was achieved by in vacuo energy minimization with the Discover algorithm (50000 steps; $\varepsilon = 1$). The backbone atoms of the TM and IL domains of the *h*-UTR were held in their position; the ligand and EL's were free to relax. Minimization was followed by a brief MD simulation period (200 ps). After this period, many poses (7 and 8 out of the 10 poses for urantide and P5U, respectively) were discarded because the ligand was driven away from its starting position and lost the salt bridge with the conserved Asp residue. The other poses (3 for urantide and 2 for P5U) converged to a very similar conformation (rmsd of the backbone atoms <1 Å), and the lowest energy complex for each ligand was chosen as starting point for subsequent 2 ns MD simulations (time step = 1 fs, T = 300 K). The backbone coordinates of the TM helices were fixed during the MD simulations because, without environmental constraints (i.e., lipid bilayer and water solution), they can move away from each other and can lose their helical structure. Fixing TM helices should still allow for sufficient spatial/conformational sampling of the docked complexes because the ligand, in the discarded poses (see above), significantly

changed both the initial position and conformation after the MD simulations. An average structure was calculated from the last 1 ns trajectory and energy-minimized using the steepest descent and conjugate gradient methods until a rmsd of 0.05 kcal/mol per Å was reached. Starting from these energy minimized structures, the model complexes of the urantide and P5U analogues **13**−**16** were obtained. The Asp[4] was replaced with a Lys or a Tic residue and the complex was minimized first relaxing only the replaced residue (10000 steps), then relaxing all the ligand (40000 steps), whereupon, a 200 ps MD simulations was performed. The average structure of the last 100 ps was reminimized until a rmsd of 0.05 kcal/mol per Å was reached. For the docking of urantide within UTR_a (switching of the ligands), we started from the optimized P5U/UTR_a complex and superposed the NMR derived urantide structure with that of P5U (backbone atoms of residues 5−10). Then, we removed the P5U structure. The complex was minimized relaxing the ligand (40000 steps). Whereupon, a 200 ps MD simulations was performed. The average structure of the last 100 ps was reminimized until a rmsd of 0.05 kcal/mol per Å was reached. Analogous steps were taken for the P5U/UTR_i complex. All the MD trajectories were analyzed by means of the Analysis module of InsightII package. Molecular graphics images of the complexes were produced using the UCSF Chimera package.[67] Rescoring of the ligand/receptor models according to the AutoDock4 (AD4)[44] scoring function was attained using a script provided within the MGLTools software package (http://mgltools.scripps.edu/).

Acknowledgment. We thank Dr. Sandro Cosconati and Dr. Michele Saviano for their helpful assistance and discussion in the preparation of this Manuscript. The LC-MS and NMR spectral data were provided by Centro di Ricerca Interdipartimentale di Analisi Strumentale, Università degli Studi di Napoli "Federico II". The assistance of the staff is gratefully appreciated. This work was supported by a grant from the Ministero dell'Istruzione, dell'Università e della Ricerca (MIUR) (PRIN 2005).

Supporting Information Available: Chemical structures of noncoded amino acids. Analytical data of the synthesized peptides. NMR data of the analyzed peptides. Details of the MD simulations. Figure of the switched complexes. Comparison of the *h*-UTR and *r*-UTR sequences. Superposition of *h*-UTR_i/β_2AR. This material is available free of charge via the Internet at http://pubs.acs.org.

References

(1) Pearson, D.; Shively, J. E.; Clark, B. R.; Geschwind, I. I.; Barkley, M.; Nishioka, R. S.; Bern, H. A. Urotensin II: A Somatostain-Like Peptide in the Caudal Neurosecretory System of Fishes. *Proc. Natl. Acad. Sci. U.S.A.* **1980**, *77*, 5021–5024.

(2) Conlon, J. M.; O'Harte, F.; Smith, D. D.; Tonon, M. C.; Vaudry, H. Isolation and Primary Structure of Urotensin II From the Brain of a Tetrapod, the Frog *Rana Ridibunda*. *Biochem. Biophys. Res. Commun.* **1992**, *188*, 578–583.

(3) Beauvillain, J. C.; Conlon, J. M.; Bern, H. A.; Vaudry, H. Cloning of the cDNA Encoding the Urotensin II Precursor in Frog and Human Reveals Intense Expression of the Urotensin II Gene in Motoneurons of the Spinal Cord. *Proc. Natl. Acad. Sci. U.S.A.* **1998**, *95*, 15803–15808.

(4) Coulouarn, Y.; Jegou, S.; Tostivint, H.; Vaudry, H.; Lihrmann, I. Cloning, Sequence Analysis and Tissue Distribution of the Mouse and Rat Urotensin II Precursors. *FEBS Lett.* **1999**, *457*, 28–32.

(5) Mori, M.; Sugo, T.; Abe, M.; Shimomura, Y.; Kurihara, M.; Kitada, C.; Kikuchi, K.; Shintani, Y.; Kurokawa, T.; Onda, H.; Nishimura, O.; Fujino, M. Urotensin II is the Endogenous Ligand of a G-protein Coupled Orphan Receptor, SENR (GPR14). *Biochem. Biophys. Res. Commun.* **1999**, *265*, 123–129.

(6) Elshourbagy, N. A.; Douglas, S. A.; Shabon, U.; Harrison, S.; Duddy, G.; Sechler, J. L.; Ao, Z.; Maleef, B. E.; Naselsky, D.; Disa, J.; Aiyar, N. V. Molecular and Pharmacological Characterization of Genes Encoding Urotensin II-Related Peptides and their Cognate G-Protein Coupled Receptors from the Mouse and Monkey. *Br. J. Pharmacol.* **2002**, *136*, 9–22.

(7) Ames, R. S.; Sarau, H. M.; Chambers, J. K.; Willette, R. N.; Aiyar, R. V.; Romanic, A. M.; Louden, C. S.; Foley, J. J.; Sauermelch, C. F.; Coatney, R. W.; Ao, Z.; Disa, J.; Holmes, S. D.; Stadel, J. M.; Martin, J. D.; Liu, W.-S.; Glover, G. I.; Wilson, S.; McNutty, D. E.; Ellis, C. E.; Eishourbagy, N. A.; Shabon, U.; Trill, J. J.; Hay, D. V. P.; Ohlstein, E. H.; Bergsma, D. J.; Douglas, S. A. Human Urotensin-II Is a Potent Vasoconstrictor and Agonist for the Orphan Receptor GPR14. *Nature* **1999**, *401*, 282–286.

(8) Sugo, T.; Murakami, Y.; Shimomura, Y.; Harada, M.; Abe, M.; Ishibashi, Y.; Kitada, C.; Miyajima, N.; Suzuki, N.; Mori, M.; Fujino, M. Identification of Urotensin II-Related Peptide as the Urotensin II Immunoreactive Molecule in the Rat Brain. *Biochem. Biophys. Res. Commun.* **2003**, *310*, 860–868.

(9) Chatenet, D.; Dubessy, C.; Leprince, J.; Boularan, C.; Carlier, L.; Segalas-Milazzo, I.; Guilhaudis, L.; Oulyadi, H.; Davoust, D.; Scalbert, E.; Pfeiffer, B.; Renard, P.; Tonon, M. C.; Lihrmann, I.; Pacaud, P.; Vaudry, H. Structure−Activity Relationships and Structural Conformation of a Novel Urotensin II-Related Peptide. *Peptides* **2004**, *25*, 1819–1830.

(10) Chartrel, N.; Conlon, J. M.; Collin, F.; Braun, B.; Waugh, D.; Vallarino, M.; Lahrichi, S. L.; Rivier, J. E.; Vaudry, H. Urotensin II in the Central Nervous System of the Frog *Rana ridibunda*: Immunohistochemical Localization and Biochemical Characterization. *J. Comput. Neurol.* **1996**, *364*, 324–339.

(11) Coulouarn, Y.; Fernex, C.; Jegou, S.; Henderson, C. E.; Vaudry, H.; Lihrmann, I. Specific Expression of the Urotensin II Gene in Sacral Motoneurons of Developing Rat Spinal Cord. *Mech. Dev.* **2001**, *101*, 187–190.

(12) Pelletier, G.; Lihrmann, I.; Vaudry, H. Role of Androgens in the Regulation of Urotensin II Precursor mRNA Expression in the Rat Brainstem and Spinal Cord. *Neuroscience* **2002**, *115*, 525–532.

(13) Pelletier, G.; Lihrmann, I.; Dubessy, C.; Luu-The, V.; Vaudry, H.; Labrie, F. Androgenic Down-Regulation of Urotensin II Precursor, Urotensin II-Related Peptide Precursor and Androgen Receptor mRNA in the Mouse Spinal Cord. *Neuroscience* **2005**, *132*, 689–696.

(14) Novellino, E.; Grieco, P.; Caraglia, M.; Budillon, A.; Franco, R.; Addeo, S. R. Peptidic and Nonpeptidic Ligands for Immunodetection of Urotensin-II Receptor PCT Int. Appl. WO 2008095995, 2008; 21 pp.

(15) Maguire, J. J.; Davenport, A. P. Is Urotensin-II the New Endothelin? *Br. J. Pharmacol.* **2002**, *137*, 579–588.

(16) Douglas, S. A.; Ohlstein, E. H. Human Urotensin-II, the Most Potent Mammalian Vasoconstrictor Identified to Date, as a Therapeutic Target for the Management of Cardivascular Diseases. *Trends Cardiovasc. Med.* **2000**, *10*, 229–237.

(17) Douglas, S. A. Human Urotensin-II as a Novel Cardiovascular Target: "Heart" of the Matter or Simply a Fish "Tail"? *Curr. Opin. Pharmacol.* **2003**, *3*, 159–167.

(18) Silvestre, R. A.; Egido, E. M.; Hernandez, R.; Leprince, J.; Chatenet, D.; Tollemer, H.; Chartrel, N.; Vaudry, H.; Marco, J. Urotensin-II is Present in Pancreatic Extracts and Inhibits Insulin Release in the Perfused Rat Pancreas. *Eur. J. Endocrinol.* **2004**, *151*, 803–809.

(19) Djordjevic, T.; Belaiba, R. S.; Bonello, S.; Pfeilschifter, J.; Hess, J.; Gorlach, A. Human Urotensin II Is a Novel Activator of NADPH Oxidase in Human Pulmonary Artery Smooth Muscle Cells. *Arterioscler. Thromb. Vasc. Biol.* **2005**, *25*, 519–25.

(20) Matsumoto, Y.; Abe, M.; Watanabe, T.; Adachi, Y.; Yano, T.; Takahashi, H.; Sugo, T.; Mori, M.; Kitada, C.; Kurokawa, T.; Fujino, M. Intracerebroventricular Administration of Urotensin II Promotes Anxiogenic-Like Behaviors in Rodents. *Neurosci. Lett.* **2004**, *358*, 99–102.

(21) Itoh, H.; McMaster, D.; Lederis, K. Functional Receptors for Fish Neuropeptide Urotensin II in Major Rat Arteries. *Eur. J. Pharmacol.* **1988**, *149*, 61–66.

(22) Flohr, S.; Kurz, M.; Kostenis, E.; Brkovich, A.; Fournier, A.; Klabunde, T. Identification of Nonpeptidic Urotensin II Receptor Antagonists by Virtual Screening Based on a Pharmacophore Model Derived from Structure−Activity Relationships and Nuclear Magnetic Resonance Studies on Urotensin II. *J. Med. Chem.* **2002**, *45*, 1799–1805.

(23) Kinney, W. A.; Almond, H. R.; Qi, J.; Smith, C. E.; Santulli, R. J.; de Garavilla, L.; Andrade-Gordon, P.; Cho, D. S.; Everson, A. M.; Feinstein, M. A.; Leung, P. A.; Maryanoff, B. E. Structure−Function Analysis of Urotensin II and its Use in the Construction of a Ligand−Receptor Working Model. *Angew. Chem., Int. Ed.* **2002**, *41*, 2940–2944.

(24) Brkovic, A.; Hattenberger, A.; Kostenis, E.; Klabunde, T.; Flohr, S.; Kurz, M.; Bourgault, S.; Fournier, A. Functional and Binding Characterizations of Urotensin II-Related Peptides in Human and Rat Urotensin II-Receptor Assay. *J. Pharmacol. Exp. Ther.* **2003**, *306*, 1200–1209.

(25) Labarrere, P.; Chatenet, D.; Leprince, J.; Marionneau, C.; Loirand, G.; Tonon, M. C.; Dubessy, C.; Scalbert, E.; Pfeiffer, B.; Renard, P.; Calas, B.; Pacaud, P.; Vaudry, H. Structure−Activity Relationships of Human Urotensin II and Related Analogues on Rat Aortic Ring Contraction. *J. Enzyme Inhib. Med. Chem.* **2003**, *18*, 77–88.

(26) Coy, D. H.; Rossowski, W. J.; Cheng, B. L.; Taylor, J. E. Structural Requirements at the N-Terminus of Urotensin II Octapeptides. *Peptides* **2002**, *23*, 2259–2264.
(27) Lescot, E.; Bureau, R.; Rault, S. Nonpeptide Urotensin-II Receptor Agonists and Antagonists: Review and Structure−Activity Relationships. *Peptides* **2007**, *29*, 680–690.
(28) Hruby, V. J. Designing Peptide Receptors Agonists and Antagonists. *Nat. Rev. Drug Discovery* **2002**, *1*, 847–858.
(29) Carotenuto, A.; Grieco, P.; Rovero, P.; Novellino, E. Urotensin-II Receptor Antagonists. *Curr. Med. Chem.* **2006**, *13*, 267–275.
(30) Grieco, P.; Carotenuto, A.; Campiglia, P.; Zampelli, E.; Patacchini, R.; Maggi, C. A.; Novellino, E.; Rovero, P. A New Potent Urotensin-II Receptor Peptide Agonist Containing a Pen Residue at Disulfide Bridge. *J. Med. Chem.* **2002**, *45*, 4391–4394.
(31) Patacchini, R.; Santicioli, P.; Giuliani, S.; Grieco, P.; Novellino, E.; Rovero, P.; Maggi, C. A. Urantide: an Ultrapotent Urotensin II Antagonist Peptide in the Rat Aorta. *Br. J. Pharmacol.* **2003**, *140*, 1155–1158.
(32) Camarda, V.; Song, W.; Marzola, E.; Spagnol, M.; Guerrini, R.; Salvatori, S.; Regoli, D.; Thompson, J. P.; Rowbotham, D. J.; Behm, D. J.; Douglas, S. A.; Calo', G.; Lambert, D. G. Urantide Mimics Urotensin-II Induced Calcium Release in Cells Expressing Recombinant UT Receptors. *Eur. J. Pharmacol.* **2004**, *498*, 83–86.
(33) Grieco, P.; Carotenuto, A.; Campiglia, P.; Marinelli, L.; Lama, T.; Patacchini, R.; Santicioli, P.; Maggi, C. A.; Rovero, P.; Novellino, E. Urotensin-II Receptor Ligands. From Agonist to Antagonist Activity. *J. Med. Chem.* **2005**, *48*, 7290–7297.
(34) Carotenuto, A.; Grieco, P.; Campiglia, P.; Novellino, E.; Rovero, P. Unraveling the Active Conformation of Urotensin II. *J. Med. Chem.* **2004**, *47*, 1652–1661.
(35) Stewart J. M.; Young J. D. *Solid Phase Peptide Synthesis*, 2nded.; Pierce Chemical: Rockford, IL, 1984.
(36) Wüthrich, K. *NMR of Proteins and Nucleic Acids*; John Wiley & Sons, Inc: New York, 1986.
(37) (a) Piantini, U.; Sorensen, O. W.; Ernst, R. R. Multiple Quantum Filters for Elucidating NMR Coupling Network. *J. Am. Chem. Soc.* **1982**, *104*, 6800–6801. (b) Marion, D.; Wüthrich, K. Application of Phase Sensitive Two-Dimensional Correlated Spectroscopy (COSY) for Measurements of $^1H-^1H$ Spin-Spin Coupling Constants in Proteins. *Biochem. Biophys. Res. Commun.* **1983**, *113*, 967–974.
(38) Braunschweiler, L.; Ernst, R. R. Coherence Transfer by Isotropic Mixing: Application to Proton Correlation Spectroscopy. *J. Magn. Reson.* **1983**, *53*, 521–528.
(39) Jenner, J.; Meyer, B. H.; Bachman, P.; Ernst, R. R. Investigation of Exchange Processes by Two-Dimensional NMR Spectroscopy. *J. Chem. Phys.* **1979**, *71*, 4546–4553.
(40) Bartels, C.; Xia, T.; Billeter, M.; Guentert, P.; Wüthrich, K. The Program XEASY for Computer-Supported NMR Spectral Analysis of Biological Macromolecules. *J. Biomol. NMR* **1995**, *6*, 1–10.
(41) Palczewski, K.; Kumasaka, T.; Hori, T.; Behnke, C. A.; Motoshima, H.; Fox, B. A.; Le Trong, I.; Teller, D. C.; Okada, T.; Stenkamp, T. E.; Yamamoto, M.; Miyano, M. Crystal Structure of Rhodopsin: A G Protein-Coupled Receptor. *Science* **2000**, *289*, 739–745.
(42) Lavecchia, A.; Cosconati, S.; Novellino, E. Architecture of the Human Urotensin II Receptor: Comparison of the Binding Domains of the Peptide and Nonpeptide Urotensin II Agonists. *J. Med. Chem.* **2005**, *48*, 2480–2492.
(43) Holleran, B. J.; Beaulieu, M. E.; Proulx, C. D.; Lavigne, P.; Escher, E.; Leduc, R. Photolabelling the Urotensin II Receptor Reveals Distinct Agonist- and Partial-Agonist-Binding Sites. *Biochem. J.* **2007**, *402*, 51–61.
(44) (a) Goodsell, D. S.; Morris, G. M.; Olson, A. J. Automated Docking of Flexible Ligands: Applications of AutoDock. *J. Mol. Recognit.* **1996**, *9*, 1–5. (b) Morris, G. M.; Goodsell, D. S.; Halliday, R. S.; Huey, R.; Hart, W. E.; Belew, R. K.; Olson, A. J. Automated Docking Using a Lamarckian Genetic Algorithm and an Empirical Binding Free Energy Function. *J. Comput. Chem.* **1998**, *19*, 1639–1662. (c) Huey, R.; Morris, G. M.; Olson, A. J.; Goodsell, D. S. Software News and Update. A Semiempirical Free Energy Force Field with Charge-Based Desolvation. *J. Comput. Chem.* **2007**, *28*, 1145–1152.
(45) Fowler, C. B.; Pogozheva, I. D.; Lomize, A. L.; LeVine, H.; Mosberg, H. I. Complex of an Active μ-Opioid Receptor with a Cyclic Peptide Agonist Modeled from Experimental Constraints. *Biochemistry* **2004**, *43*, 15796–15810. http://mosberglab.phar.umich.edu/resources/models/OPSD_BOVIN_AD.pdb.
(46) Marzola, E.; Camarda, V.; Batuwangala, M.; Lambert, D. G.; Caló, G.; Guerrini, R.; Trapella, C.; Regoli, D.; Tomatis, R.; Salvadori, S. Structure−Activity Relationship Study of Position 4 in the Urotensin-II Receptor Ligand U-II(4−11). *Peptides* **2008**, *29*, 674–679.
(47) Moroder, L.; Romano, R.; Guba, W.; Mierke, D. F.; Kessler, H.; Delporte, C.; Winand, J.; Christophe, J. New Evidence for a Membrane Bound Pathway in Hormone Receptor Binding. *Biochemistry* **1993**, *32*, 13551–13559.
(48) Sargent, D. F.; Schwyzer, R. Membrane Lipid Phase as Catalyst for Peptide−Receptor Interactions. *Proc. Natl. Acad. Sci. U.S.A.* **1986**, *83*, 5774–5778.
(49) Lescot, E.; Sopkova-de Oliveira Santos, J.; Colloc'h, N.; Rodrigo, J.; Milazzo-Segalas, I.; Bureau, R.; Rault, S. Three-Dimensional Model of the Human Urotensin-II Receptor: Docking of Human Urotensin-II and Nonpeptide Antagonists in the Binding Site and Comparison with an Antagonist Pharmacophore Model. *Proteins* **2008**, *73*, 173–184.
(50) Cherezov, V.; Rosenbaum, D. M.; Hanson, M. A.; Rasmussen, S. G.; Thian, F. S.; Kobilka, T. S.; Choi, H. J.; Kuhn, P.; Weis, W. I.; Kobilka, B. K.; Stevens, R. C. High-Resolution Crystal Structure of an Engineered Human Beta2-Adrenergic G Protein-Coupled Receptor. *Science* **2007**, *318*, 1258–1265.
(51) Warne, T.; Serrano-Vega, M. J.; Baker, J. G.; Moukhametzianov, R.; Edwards, P. C.; Henderson, R.; Leslie, A. G.; Tate, C. G.; Schertler, G. F. Structure of a Beta1-Adrenergic G-Protein-Coupled Receptor. *Nature* **2008**, *454*, 486–491.
(52) Jaakola, V. P.; Griffith, M. T.; Hanson, M. A.; Cherezov, V.; Chien, E. Y.; Lane, J. R.; Ijzerman, A. P.; Stevens, R. C. The 2.6 Angstrom Crystal Structure of a Human A2a Adenosine Receptor Bound to an Antagonist. *Science* **2008**, *322*, 1211–1217.
(53) Boivin, S.; Guilhaudis, L.; Milazzo, I.; Oulyadi, H.; Davoust, D.; Fournier, A. Characterization of Urotensin-II Receptor Structural Domains Involved in the Recognition of U-II, URP, and Urantide. *Biochemistry* **2006**, *45*, 5993–6002.
(54) Boivin, S.; Ségalas-Milazzo, I.; Guilhaudis, L.; Oulyadi, H.; Fournier, A.; Davoust, D. Solution Structure of Urotensin-II receptor Extracellular Loop III and Characterization of its Interaction with Urotensin-II. *Peptides* **2008**, *29*, 700–710.
(55) Boucard, A. A.; Sauvé, S. S.; Guillemette, G.; Escher, E.; Leduc, R. Photolabelling the Rat Urotensin II/GPR14 Receptor Identifies a Ligand-Binding Site in the Fourth Transmembrane Domain. *Biochem. J.* **2003**, *370*, 829–838.
(56) Guerrini, R.; Camarda, V.; Marzola, E.; Arduin, M.; Calo, G.; Spagnol, M.; Rizzi, A.; Salvatori, S.; Regoli, D. Structure−Activity Relationship Study on Human Urotensin II. *J. Pept. Sci.* **2005**, *11*, 85–90.
(57) Camarda, V.; Spagnol, M.; Song, W.; Vergura, R.; Roth, A. L.; Thompson, J. P.; Rowbotham, D. J.; Guerrini, R.; Marzola, E.; Salvatori, S.; Cavanni, P.; Regoli, D.; Douglas, S. A.; Lambert, D. G.; Calò, G. In Vitro and In Vivo Pharmacological Characterization of the Novel UT Receptor Ligand [Pen5, DTrp7, Dab8]Urotensin II(4−11) (UFP-803). *Br. J. Pharmacol.* **2006**, *147*, 92–100.
(58) Misika, A.; Hruby, V. J. Optimization of Disulfide Bond Formation. *Pol. J. Chem.* **1994**, *68*, 893–899.
(59) (a) Kenakin, T. P. Competitive antagonism. In *Pharmacologic Analysis of Drug−Receptor Interaction*, 3rd ed.; Lippincott-Raven Press: Philadelphia, 1997; pp 331−373. (b) Cheng, Y.; Prusoff, W. H. Relationship Between the Inhibition Constant (K_i) and the Concentration of Inhibitor Which Causes 50 Percent Inhibition (I_{50}) of an Enzymatic Reaction. *Biochem. Pharmacol.* **1973**, *22*, 3099–3108.
(60) Hwang, T. L.; Shaka, A. J. Water Suppression that Works. Excitation Sculpting Using Arbitrary Wave-Forms and Pulsed-Field Gradients. *J. Magn. Reson.* **1995**, *112*, 275–279.
(61) Mueller, L. P. E. COSY, a Simple Alternative to E. COSY. *J. Magn. Reson.* **1987**, *72*, 191–196.
(62) States, D. J.; Haberkorn, R. A.; Ruben, D. J. A Two-Dimensional Nuclear Overhauser Experiment with Pure Absorption Phase in Four Quadrants. *J. Magn. Reson.* **1982**, *48*, 286–292.
(63) Guntert, P.; Mumenthaler, C.; Wüthrich, K. Torsion Angle Dynamics for NMR Structure Calculation with the New Program, DYANA. *J. Mol. Biol.* **1997**, *273*, 283–298.
(64) Koradi, R.; Billeter, M.; Wüthrich, K. MOLMOL: A Program for Display and Analysis of Macromolecular Structures. *J. Mol. Graphics* **1996**, *14*, 51–55.
(65) Maple, J.; Dinur, U.; Hagler, A. T. Derivation of Force Fields for Molecular Mechanics and Dynamics from Ab Initio Energy Surface. *Proc. Natl. Acad. Sci. U.S.A.* **1988**, *85*, 5350–5354.
(66) (a) Laskowski, R. A.; MacArthur, M. W.; Moss, D. S.; Thornton, J. M. PROCHECK: A Program to Check the Stereochemical Quality of Protein Structures. *J. Appl. Crystallogr.* **1993**, *26*, 283–291. (b) Morris, A. L.; MacArthur, M. W.; Hutchinson, E. G.; Thornton, J. M. Stereochemical Quality of Protein Structure Coordinates. *Proteins* **1992**, *12*, 345–364.
(67) Pettersen, E. F.; Goddard, T. D.; Huang, C. C.; Couch, G. S.; Greenblatt, D. M.; Meng, E. C.; Ferrin, T. E. UCSF Chimera−A Visualization System for Exploratory Research and Analysis. *J. Comput. Chem.* **2004**, *25*, 1605–1612.

JM900148C